Copy No. _____

Defence Research and Development Canada
Recherche et développement pour la défense Canada

DEFENCE R&D DÉFENSE

Aural classification and temporal robustness

Stefan M. Murphy
Paul C. Hines

Defence R&D Canada – Atlantic

Technical Report
DRDC Atlantic TR 2010-136
November 2010

Canada

This page intentionally left blank.

Aural classification and temporal robustness

Stefan M. Murphy
Paul C. Hines

Defence R&D Canada – Atlantic
Technical Report
DRDC Atlantic TR 2010-136
November 2010

Principal Author

Original signed by Stefan M. Murphy

Stefan M. Murphy

Defence Scientist

Approved by

Original signed by Garry Heard for

Daniel Hutt

Head/Underwater Sensing

Approved for release by

Original signed by Ron Kuwahara for

Calvin Hyatt

Head/Document Review Panel

Abstract

Active sonar systems are used to detect underwater manmade objects of interest (*targets*) that are too quiet to be reliably detected with passive sonar. In coastal waters, the performance of active sonar is degraded by false alarms caused by echoes returned from geological seabed structures (*clutter*) found in these shallow regions. To reduce false alarms, a method of distinguishing target echoes from clutter echoes is required. Research has demonstrated that perceptual signal features similar to those employed in the human auditory system can be used to automatically discriminate between target and clutter echoes, thereby improving sonar performance by reducing the number of false alarms.

An active sonar experiment on the Malta Plateau was conducted during the Clutter07 sea trial and repeated during the Clutter09 sea trial. Broadband sources were used to transmit linear FM sweeps (600–3400 Hz) and a cardioid towed-array was used as the receiver. The dataset consists of over 95 000 pulse-compressed echoes returned from two targets and many geological clutter objects.

These echoes are processed using an automatic classifier that quantifies the timbre of each echo using a number of perceptual signal features. Using echoes from 2007, the aural classifier is trained to establish a boundary between targets and clutter in the feature space. Temporal robustness is then investigated by testing the classifier on echoes from the 2009 experiment.

Résumé

Les sonars actifs servent à détecter sous l'eau des objets d'intérêt artificiels (cibles) trop silencieux pour être détectés efficacement par un sonar passif. En eaux côtières, les échos provenant de structures géologiques du fond marin (clutter) causent des fausses alarmes qui altèrent les performances des sonars actifs dans ces eaux peu profondes. Une méthode permettant de distinguer les échos de cibles et les échos de clutter est nécessaire pour réduire le taux de fausses alarmes. Des recherches ont montré que des caractéristiques perceptuelles du signal, semblables à celles utilisées par l'oreille humaine, peuvent servir à distinguer automatiquement entre les échos des cibles et le clutter, ce qui permet d'améliorer le rendement du sonar en réduisant le nombre de fausses alarmes. Une expérience a été effectuée au moyen d'un sonar actif sur le plateau de Malte au cours des essais en mer Clutter07 et Clutter09. Des sources à large bande ont servi à émettre des balayages FM linéaires (de 600 à 3 400 Hz), et un réseau remorqué cardioïde a servi de récepteur. L'ensemble de données est composé de plus de 95 000 échos à compression d'impulsion provenant de cibles actives et de nombreux objets géologiques produisant le clutter.

Les échos sont traités à l'aide d'un classificateur auditif automatique qui quantifie la sonorité de chaque écho à partir d'un nombre de caractéristiques perceptuelles du signal. On

entraîne le classificateur à établir, à partir d'échos de l'essai de 2007, la limite entre les cibles et le clutter dans l'espace de caractéristiques. La robustesse temporelle est ensuite examinée en faisant l'essai du classificateur au moyen d'échos de l'essai de 2009.

Executive summary

Aural classification and temporal robustness

Stefan M. Murphy, Paul C. Hines; DRDC Atlantic TR 2010-136; Defence R&D Canada – Atlantic; November 2010.

Background: The project's aim is to develop a robust classifier using aural-based features that can discriminate active sonar target echoes from unwanted clutter echoes.

Principal results: The temporal robustness of the aural classifier was examined by training the classifier using data collected during a 2007 field trial (Clutter07) and testing it on data collected during a 2009 field trial (Clutter09.) One of the most useful metrics to rate classifier performance is the area under the receiver-operating-characteristic (ROC) curve, A_{ROC}. The A_{ROC} evaluated for a classifier is 1.0 for perfect classification and 0.5 for random guessing. The ROC curve for the aural classifier in testing yields a value of $A_{\mathrm{ROC}} = 0.903$, indicative of a very successful, and in this case a temporally robust, classifier.

Significance of results: Military sonar systems must detect, localize, classify, and track submarine threats from distances safely outside their circle of attack. Active sonar operating at low frequency is favoured for the long range detection of quiet targets. However, in coastal waters, operational sonars frequently mistake echoes from geological features (clutter) for targets of interest. This results in high false alarm rates and degradation in sonar performance. Conventional approaches, using signal features based on the echo spectra or using signal features derived from physics-based models of specific target types, have had only limited success; moreover, they ignore a potentially valuable tool for target-clutter discrimination – the human auditory system. That said, even if aural discrimination is possible, discriminating targets from clutter is labour intensive and requires near-fulltime effort from the operator. Automation of on-board systems such as automated aural classification is essential since future military platforms will have to support smaller complements, and near-future operations will have to accommodate additional mission-specific forces. The technique is well suited to autonomous systems since a much smaller telemetry bandwidth is needed to transmit a classification result than to transmit raw acoustic data.

Future work: Investigation of signal-to-noise ratio (SNR) dependence on classification performance is ongoing. Understanding SNR dependence may provide insight on how to best approach the low SNR (hard case) classification problem.

Sommaire

Aural classification and temporal robustness

Stefan M. Murphy, Paul C. Hines ; DRDC Atlantic TR 2010-136 ; R & D pour la défense Canada – Atlantique ; novembre 2010.

Contexte : Le présent projet vise le développement d'un classificateur robuste qui utilise des caractéristiques basées sur l'audition pour distinguer les échos de cibles sonar actifs et les échos brouilleurs de clutter.

Résultats principaux : Nous avons examiné la robustesse temporelle du classificateur auditif en l'entraînant au moyen de données recueillies lors d'un essai en mer en 2007 (Clutter07) et le testant au moyen de données recueillies lors d'un essai en mer en 2009 (Clutter09.) L'un des paramètres les plus utiles pour coter les performances d'un classificateur est l'aire sous la courbe caractéristique de fonctionnement du récepteur (ROC), A_{ROC}. L'A_{ROC} évaluée pour un classificateur est de 1,0 pour un classement parfait et de 0,5 pour un classement aléatoire. La courbe ROC pour le classificateur auditif à l'essai a donné une valeur d'$A_{\mathrm{ROC}} = 0{,}903$, ce qui indique un classificateur très efficace, et dans ce cas-ci, temporellement robuste.

Portée des résultat : Les sonars militaires doivent détecter, localiser, classifier et poursuivre les menaces sous-marines à des distances de sécurité à l'extérieur de leur cercle d'attaque. Les sonars actifs à basse fréquence sont préférables en raison de leurs longues distances de fonctionnement contre les cibles silencieuses. Toutefois, en eaux côtières, les échos provenant d'éléments géologiques (clutter) sont souvent confondus avec des cibles d'intérêt par les sonars opérationnels. Il en résulte un taux de fausses alarmes élevé et une altération des performances du sonar. Les approches traditionnelles – l'utilisation de caractéristiques du signal fondées sur le spectre des échos ou calculées au moyen d'un modèle physique de certains types de cibles – n'ont eu qu'un succès limité ; de plus, elles négligent un outil qui pourrait s'avérer très utile pour distinguer les cibles du clutter : l'oreille humaine. Cela dit, bien que la discrimination auditive soit possible, la discrimination des cibles et du clutter demeure laborieuse et nècessite les efforts de l'opérateur presque à plein temps. Comme les futures plateformes militaires devront être dotées d'effectifs réduits et que les opérations devront dans un proche avenir répondre aux besoins de forces supplémentaires pour des missions déterminées, l'automatisation des systèmes de bord, comme la classification auditive automatique, est essentielle. Cette technique convient bien aux systèmes autonomes, car la transmission d'un résultat de classification exige une largeur de bande beaucoup plus restreinte que la transmission de données acoustiques brutes.

Recherches futures : Les recherches sur les effets du rapport signal sur bruit (S/B) sur les performances de classification se poursuivent. La compréhension des effets du rapport S/B aidera peut-être à déterminer la meilleure méthode pour aborder le problème de classification dans le cas d'un faible rapport S/B (cas difficile).

Acknowledgements

The authors would like to thank Doug Abraham, Charlie Gaumond, and Richard Menis for their participation in the Clutter09 sea trial. The Chief Scientist of the sea trial was Peter Nielson and the trial was conducted by NATO Undersea Research Centre (NURC) and the crew of NATO Research Vessel (NRV) ALLIANCE.

The authors would also like to thank the United States Office of Naval Research for partial funding provided for this work.

Table of contents

List of figures

List of tables

This page intentionally left blank.

1 Introduction

Active sonar systems are used to detect underwater manmade objects of interest (*targets*) that are too quiet to be reliably detected with passive sonar. In shallow coastal waters, active sonar performance is degraded by false alarms caused by echoes returned from geological seabed structures (*clutter*). To reduce false alarms, a method of distinguishing target echoes from clutter echoes is required.

Sonar operators are capable of distinguishing targets from clutter by listening to their echoes, and acheived high classification performance in a human listening experiment at DRDC [1]. Following the experiment, DRDC developed an *automatic aural classifer* to mimic the human listening process in order to automate this capability of sonar operators [2]. The classifier uses aural features – perceptual features derived from timbre – to describe the echoes, and looks for trends in the features that allow the target echoes to be separated from clutter.

Echo signals are affected by unstable environmental factors such as background noise and sound propagation conditions. Because these factors are temporally variable, they can cause differences in (otherwise identical) echoes received from pings sent out at different times. Therefore, the aural features that describe the echoes must be temporally robust – insensitive to changes in echoes from varying conditions – in order to train the aural classifier in advance and then successfully classify echoes received after a lapse of time.

To investigate temporal robustness, an active sonar experiment was performed on the Malta Plateau during a sea trial that took place in 2007 (Clutter07), and was repeated during a sea trial in 2009 (Clutter09). The aural classifier is trained using target and clutter echoes from the Clutter07 sea trial and then tested by performing classification on echoes from the Clutter09 sea trial. The active sonar experiments performed during the sea trials were very similar. In both experiments, a research ship followed the same route and transmitted linear frequency modulated (LFM) pings. Using a towed array, echoes from each ping were received from clutter, as well as from two manmade objects in the area which were used as targets: the oil rig and the wellhead belonging to Campo Vega Oilfield. Over 95,000 echoes were collected, forming a database nearly two orders of magnitude larger than databases used in previous studes [2, 3]. Although the experiments were conducted in the same location, they were separated by two years, and the environmental conditions were considerably different. This provides an excellent dataset with which to evaluate the temporal robustness of the classifier.

In Section 2, details of the Clutter07 and Clutter09 experiments are reviewed and differences highlighted. Section 3 details the processing of data collected during the two experiments in order to extract target and clutter echoes. A brief background on the aural classifier is provided in Section 4. Section 5 presents the classification results, and conclusions are highlighted in Section 6.

2 The experiments

In order to establish a database of active sonar echoes for evalutation of the aural classifier, two active sonar experiments were performed two years apart: the first during the Clutter07 sea trial, and a second during the Clutter09 sea trial. Section 2.1 reviews the procedure common to both experiments including the ship track and location, and provides some detail on the common format for data collection. Section 2.2 highlights the experimental differences between trials that have implications on the aural characteristics of the sonar echoes.

2.1 Procedure

Although the Clutter07 and Clutter09 sea trials each hosted several experiments, the experiments considered in this study took place on May 29, 2007 and approximately two years later on May 3, 2009. Both trials took place on the Malta Plateau, between Malta and Sicily, and in each experiment, NATO Research Vessel (NRV) ALLIANCE ran the track shown as the yellow dashed line in Figure 1. Time stamped waypoints for the ship tracks in Clutter07 and Clutter09 are listed in Tables A.1 and A.2 in Annex A. Note the position of Campo Vega Oilfield southeast of the starting point of the track. The wellhead is located approximately 2.5 km north-northeast of the oil rig. Both tracks started mid-morning and ran for about eight hours with an average ship speed of approximately 5 knots.

While NRV ALLIANCE ran its track, linear frequency modulated (LFM) upsweeps of duration 1.1 seconds from 500–3500 Hz were transmitted every two minutes using the NATO Undersea Research Centre (NURC) low-frequency and mid-frequency towed free-flooding ring sources. To avoid damaging the projectors with abrupt voltage changes, the LFMs were ramped up in power from 500–600 Hz and ramped down from 3400–3500 Hz. Since both sources were required to cover the full bandwidth, the transmitted sweep transitioned from the low-frequency source to the mid-frequency source over the 1800–1820 Hz band. NURC's cardioid towed array was used as the receiver.

Non-acoustic data were also recorded, of which relevant measurements include: Global Positioning System (GPS) data (latitude, longitude, and speed over ground), and the compass heading of the towed array. These data are averaged over 60 seconds following the ping transmission to provide a more stable estimate of the towed array position relative to the ship, and because echoes were recorded for 55 seconds following the transmission. Due to large bearing errors, the data recorded during ship turning manoeuvre are omitted. The omitted ping times are listed in Tables A.1 and A.2 in Annex A.

Additional experimental details are listed in Annex B.

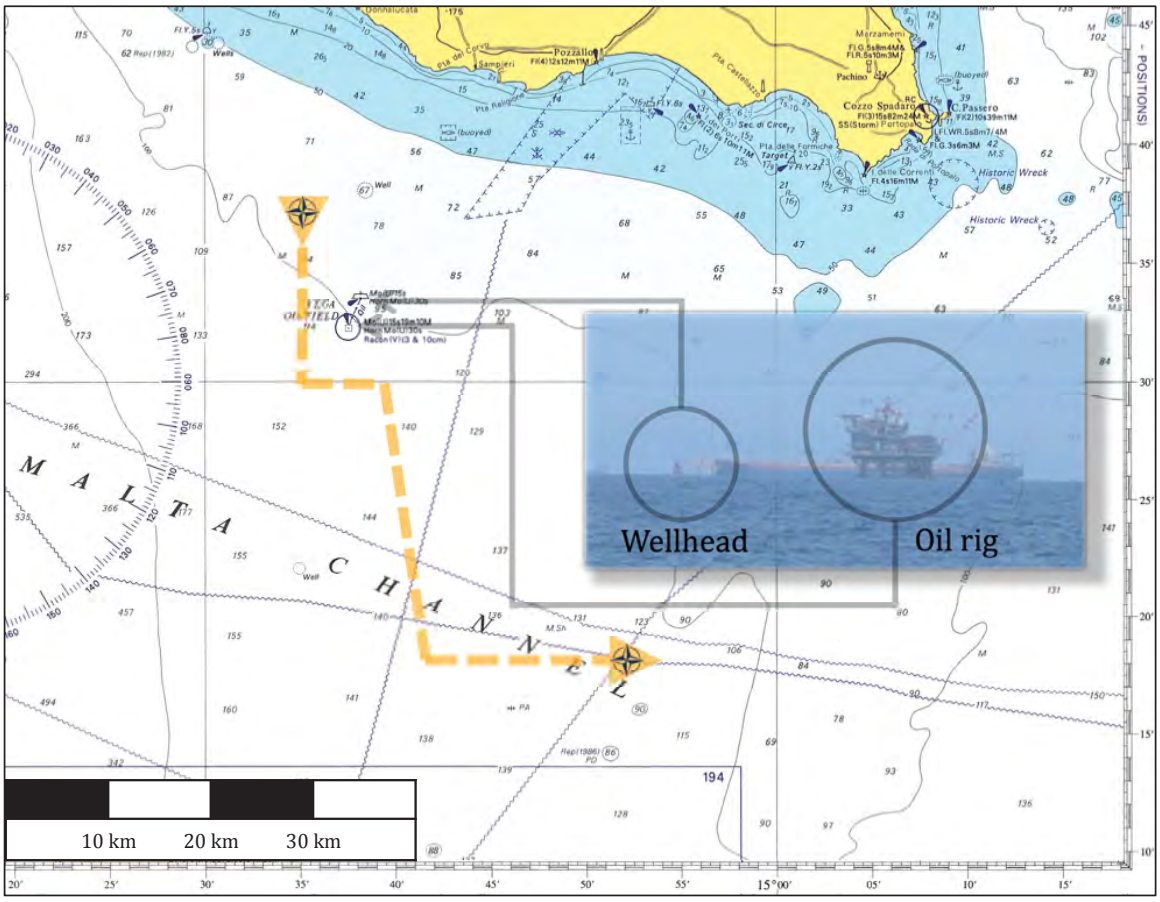

Figure 1: *NRV ALLIANCE's track (yellow dashed line) on the Malta Plateau. A photo of Campo Vega Oilfield's rig and wellhead (located just southeast of the track start point) is included.*

2.2 Experimental differences

There were some substantial differences between the 2007 and 2009 experiments, even though factors such as the procedure, location, and season were kept constant. Although many factors such as geological changes and marine life are difficult to quantify, there were two measurable differences between the 2007 and 2009 experiments.

First, the weather conditions differed considerably. During the experiment in Clutter07 the average wind speed was 15.2 knots, while the average wind speed during the Clutter09 experiment was only 3.8 knots. Photographs of Campo Vega from each experiment are shown in Figure 2 and a significant difference in sea state can be observed; Beaufort force 5–6 seas were present in 2007 whereas nearly calm seas (Beaufort force 1) were present in 2009. The reduction in sea state from 2007 to 2009 leads to a decrease in wind-driven ambient noise. Calmer seas also lead to a decrease in surface scatter since the roughness of

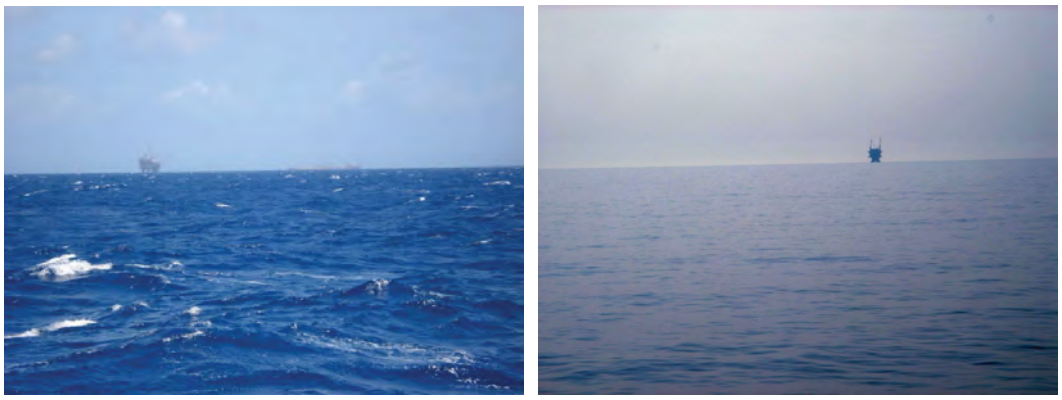

(a) (b)

Figure 2: *Campo Vega viewed from ALLIANCE in 2007 (a) and 2009 (b). Note the decrease in sea state from 2007 to 2009.*

the surface and number of air bubbles caused by breaking waves is decreased. For example, at the center frequency of the LFM (2000 Hz), the backscattering strength computed in [4] is approximately 30 dB lower at a wind speed of 5 knots than it is at 20 knots at a grazing angle of 10°.

Second, although both trials occurred during the month of May, the sound speed profiles were significantly different (Figure 3). For reference, NRV ALLIANCE's sources and receiver were towed at a depth of approximately 50 m during both sea trials. The profiles are calculated from expendable bathythermograph (XBT) data taken near Waypoint 7 in Tables A.1 and A.2.

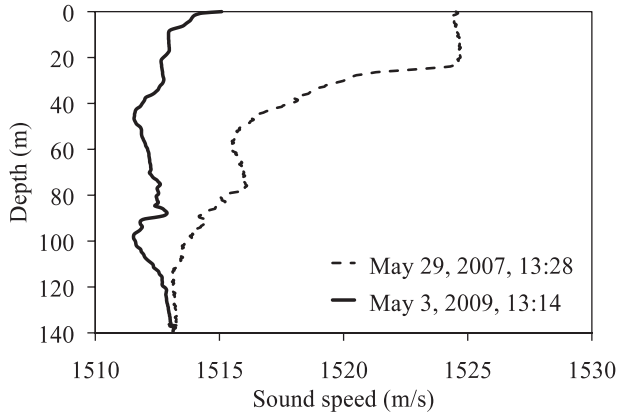

Figure 3: *Sound speed profiles from XBT data collected on NRV ALLIANCE.*

While the 2007 sound speed profile is downward refracting, the 2009 profile is nearly isospeed. The differences in the sound speed profiles and surface reflections contribute to different sound propagation conditions for each trial; these could alter received echo signals and the aural features that describe them.

3 Data processing

This section documents the details of the data processing, starting with the beamformed data acquired on NRV ALLIANCE, and ending with individual echoes with known identities, confirmed to have been returned from the Campo Vega oil rig or wellhead, or clutter. The processing procedure was developed for the Clutter09 sea trial, and used to process data from both Clutter07 and Clutter09 experiments for consistency.

3.1 Echo detection and extraction

The author of [5] developed a detector for Clutter09 based on the normalization scheme implemented in that paper. An overview of the detector is now presented, while a detailed description of the detector and a discussion on reverberation statistics can be found in Annex C. In the first stage of the detector, the beamformed data from NURC's cardioid array are *matched-filtered* using a replica of the LFM transmitted. The *envelope* is then computed by taking the magnitude of the analytic signal. *Squaring* the envelope results in reverberation intensity data, which are then *normalized* using a split-window normalizer [5] to flatten the reverberation decay. Detections are identified as samples in the normalized intensity data that exceed a defined threshold (see Appendix C). The detector employs a clustering algorithm in range and bearing to reduce the number of redundant detections – multiple exceedances associated with a single echo. Across bearing, redundant detections are caused by signal leakage into sidelobes, while in range multiple detections can be caused by multipath arrivals or by arrival time differences due to the physical extent of individual reflectors.

The detections found by the detector are used to extract matched-filtered echoes from the time series for classification. Ideally, detection and echo extraction would occur in the same process; however, the detector and extraction application were developed independently as a collaborative effort in analyzing the Clutter09 data. The detector applies a matched-filter to the beamformed time series using a simple parameter-generated replica, which does not account for the Doppler effect introduced by the speed of advance of the ship. To maximize signal-to-noise ratio (SNR) before echo extraction, the original beamformed time series are matched-filtered using Doppler shifted versions of the actual LFM waveform transmitted. Each beam is matched-filtered with a custom Doppler shifted replica that takes into account the beam angle and the array tow speed at the time of ping transmission. Details of this Doppler processing are documented in [6].

Echoes are then extracted by forming a 1.0 second Waveform Audio File Format (WAV) file from the Doppler-corrected (matched-filtered time series) data 0.5 seconds before and after the detection sample.

3.2 Echo identification

In order to have useful data for training and testing the classifier, each extracted echo needs to be labelled as being returned from the oil rig, wellhead, or clutter[1]. Due to the large number of echoes, most of this process has been automated; however, some manual refining, as explained in Section 3.2.2, is done to verify the automatic labelling.

3.2.1 Automated identification procedure

The contact location associated with each echo is determined from the range (time delay) and the bearing angle (beam number) of the detection. The bearing uncertainty is the largest contributor to the contact location error, since the beam width is as high as 14.8° at the end-fire beam angle. Bearing accuracy could be improved by interpolating between beams using the beam pattern, but this has not been implementeds

The coordinates of the oil rig and wellhead (targets) are known (see Appendix B), but due to the sonar's range and bearing resolution, and to ensure that no target echoes were missed, all contacts within 2.4 km of each target position are considered as candidates for association with that target. This distance corresponds to the separation between the oil rig and wellhead. All other echoes are considered to be clutter. Additional precautions were taken in order to ensure the oil rig and wellhead contact labels were not reversed: if a contact was within range of both the oil rig and wellhead, the contact was assigned to the closer object.

The large distance threshold resulted in many clutter echoes being associated with each of the targets, which necessitated manual refining of the labels following the process described in the next section.

3.2.2 Manual identification refining

Each ping produces at most one valid echo from each of the targets; however, the automatic identification process can assign many contacts to a target for single ping, and these mislabelled echoes must be corrected manually. This is accomplished by listening to the echoes to make sure they sound similar to echoes already designated with the same label. To avoid relying only on the listening test with its human factor uncertainty, each echo's SNR, time delay, and beam number are also considered. For each of the targets' echoes, the values for SNR, time delay, and beam number varied predictably over consecutive pings since the ship travelled at a constant speed. Echoes with large discrepancies in the values expected from the previous ping(s) could be quickly identified as clutter.

[1] Although not considered in this study, echoes from a passive acoustic target deployed in both experiments also need to be identified so they can be isolated from the dataset.

The manual refining process ensured that the wellhead and oil rig had, at most, one echo, and there was a high degree of confidence that it was correctly labelled. The process also made sure that all of the echoes from the wellhead and oil rig were accounted for, and not mislabelled as clutter. Pings with missing target echoes that were expected to be present based on high SNRs observed in time-adjacent pings were investigated and recovered from mislabelled clutter echoes in some cases.

3.3 Database expansion with off-beam target echoes

The database containing echoes with known identities is highly valuable; however, it can be further improved to address two limitations. First, the number of clutter echoes extracted is much greater than the number of target echoes. This is typical for active sonar; however, unbiased classification testing requires an equal number of target and clutter echoes. Second, the SNR of the target echoes is typically greater than that of the clutter echoes for the Clutter07 and Clutter09 data. To avoid classification biasing, they should have similar SNR. In Section 5.1, the number of target and clutter echoes is made equal, and the SNR distributions are matched, so that classification is not biased by prior probabilities (relative number of clutter and target echoes) or by SNR.

There are a number of ways to accomplish matching the target and clutter population sizes and SNRs. The number of clutter echoes could be limited to a relatively small number of high SNR examples to match the population of target echoes. This would discard the majority of the clutter data, and would not test the classifer on low SNR echoes – an important aspect of its performance. A better solution is to obtain a large number of lower SNR target echoes by selecting off-beam instances of echoes from sidelobe leakage that were initially removed by the beam clustering of the detector. This technique was used in [3], and in the present application it increases the number of target echoes by two orders of magnitude, while at the same time obtaining a broader SNR distribution.

There is one technical detail that should be noted regarding this technique: particular attention must be paid to the Doppler effect when extracting off-beam echoes. Recall that the matched-filter used in the echo extraction process correlates each beam with a custom Doppler-shifted replica that takes into account the ship's radial velocity on that beam[1]. Off-beam echoes are caused by leakage from the main beam signal, and although they may be measured on a number of beams, they have propagated to the receiver from a single bearing. Therefore, in extracting off-beam echoes, every beam is corrected for Doppler using the same Doppler shift measured on the main beam, rather than using a different replica for each beam as in the initial processing. This ensures that echo features are not affected by improper Doppler correction, which is important for aural classification.

[1]The radial velocity is the rate of change of the distance between the ship and the contacts on a particular beam and is calculated using the beam angle. For example, the magnitude of the radial velocity is equal to the ship speed on end-fire beams, and is zero on broadside beams.

4 Aural classifier

The aural classifier mimics the human auditory system by conditioning signals (i.e., active sonar echoes) in a similar way as the outer and inner human ear, and by simulating the cognitive process through representing the echoes as perceptual features. A Gaussian classifier that uses Bayes decision theory then simulates the human decision-making process, in this case to determine whether an echo should be designated as a target or as clutter. A brief overview of the aural feature calculation is given in Section 4.1, while a full description of the specific features is detailed in [3]. Methods for reducing the feature dimensionality are considered in Section 4.2 to address the problems assosicated with limited numbers of samples. The generic Gaussian classifier is reviewed in Section 4.3, and metrics for evaluating its performance are presented in Section 4.4.

4.1 Aural feature calculation

The human auditory system mimiced by the aural classifier can be separated into 2 processes: the mechanical process that conditions signals incident on the ear, and the cognitive process in which the brain perceives the nerve signals generated from the incident mechanical signals.

The first stage of the auditory system is mimiced by processing echoes with a model of the mechanical response of the human ear. An auditory filter bank produces approximately 50 bandpass-filtered versions of the original echo, representing the narrow-band responses at locations along the cochlea (inner ear) that are excited at different frequencies. In the human ear, the basilar membrane converts these mechanical responses into nerve signals which are used by the cognitive process.

The cognitive process is extremely complex and cannot be captured in a model. In order to account for this process and create a perceptual representation of each echo, the classifier extracts features derived from *timbre* which is used to describe perceptual features in the field of musical acoustics. These perceptual-based quantities (i.e., attack time, duration, loudness, etc.) are calculated for all of the bandpass-filtered versions of each echo, and summary statistics including the minimum, maximum, and mean, are used to produce 58 *aural features*. The reader is referred to [3] for a detailed description of the aural features.

Some features may be redundant if they are highly correlated over the echoes in a particular dataset under evaluation. In other words, if a feature value is known for a given echo, and the value of a different feature can be simply calculated from the first feature value, then one of the features is redundant. Redundant features do not provide additional information on the echoes and are therefore removed from consideration. There are typically less than 20 redundant features for datasets of echoes from the Clutter07 and Clutter09 databases. This leaves over 30 non-redundant features that are reduced to a smaller number of dimensions

in the next section in order to permit their implementation in a practical manner.

4.2 Feature dimension reduction

4.2.1 Curse of dimensionality

The aural classifier assumes that the aural feature values are Gaussian distributed, and this will be discussed further in Section 4.3. A sample population from any statistical distribution requires adequate spatial density of samples in order to accurately represent the distribution. As the dimensionality of each sample increases, the number of samples must increase exponentially to maintain a constant sampling density. This is known as the *curse of dimensionality*. If N is the number of samples required for a dense population in a single dimension, N^p is the sample size required to maintain a dense population in p dimensions [7]. For simplicity, imagine that a Gaussian distribution can be densely represented by only 10 samples in one dimension. In order to maintain population density in 58 dimensions (the number of features used by the classifier), the sample size needs to be 10^{58}, which is impractical. Clearly one must reduce the feature dimensionality. Sample sizes encountered in this study are relatively large, but do not exceed the order of 10,000 echoes. Even if 10 samples were adequate in a single dimension, the number of dimensions should not exceed 4, since $10^4 = 10,000$. *Feature selection* and *principal component analysis* are techniques used to reduce dimensionality, and although the (optimistic) maximum number of 4 dimensions is not taken to be a restriction in this work, it should be kept in mind.

4.2.2 Feature selection

Currently, the aural classifier reduces the number of non-redundant features by individually ranking them based on how well they can discriminate between targets and clutter in the training dataset. The number of features kept is user defined and is typically less than 15. There are various methods of ranking features, and two are considered in this study: the *overlap fraction* of class probability density functions, and *discriminant score*.

4.2.2.1 Overlap fraction

For a given feature, the overlap fraction method calculates the mean and variance of each class over the entire training dataset. Using these parameters, a Gaussian probability density function (pdf) is constructed for each class, and the fraction of the total area under the pdfs common to all of the classes is calculated. Intuitively, low overlap fractions indicate features with separation between classes. One potential downside of this method is that it allows features with identical means to achieve high ranking if they have large differences in their variances, as depicted in Figure 4. Although discrimination by variance alone is not unreasonable, explicitly including separation of means in the ranking metric is more intuitive, and this is the approach is taken in discriminant analysis.

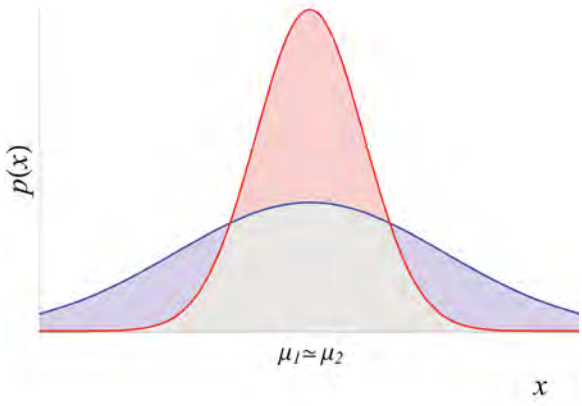

Figure 4: *The overlap region of two class pdfs (Gaussian) is coloured gray. The overlap fraction equals the area of the overlap region, which is in the range* $[0,1]$ *since the area under a pdf is equal to 1. In this example, the overlap fraction is relatively small* (≈ 0.5) *even though the class means are equal.*

4.2.2.2 Discriminant score

Discriminant analysis finds projection directions (linear combinations of d-dimensions to form a scalar) that are best for discrimination between classes. For a c-class problem, the projection is from d-dimensional space to $(c-1)$-dimensional space where $d \geq c$ [8]. The current application, based on discriminant analysis, ranks features *individually* so that the d-dimensional feature space is ranked and sorted rather than projected to a lower dimensional space.

In the case of a binary classifier, the discriminant score, s_D, is calculated for each feature:

$$s_D = \frac{(\mu_1 - \mu_2)^2}{(\sigma_1 + \sigma_2)^2} \tag{1}$$

where μ_i is the mean value of each class for the given feature, and $\sigma_i = \sqrt{\sigma_i^2}$ is the standard deviation (square root of the variance) of each class. A feature that is well separated between classes has a large difference in class means relative to a measure of the total variance. This scoring value is similar to the criterion function that is maximized in linear discriminant analysis to determine the optimal direction of projection [8]. Here, since each feature is considered individually and the optimization approach is not taken, a single value rather than a projection vector is calculated.

The discriminant score has a meaningful value. Consider Figure 5, which depicts variations of two theoretical Gaussian pdfs representing the distributions of a single feature for

two classes (shown in blue and red) at different degrees of separation. Figure 5(a) shows distributions with poor separation, and Figure 5(c) shows distributions with good separation. In Figure 5(b), the classes are at a natural limit of separation: neither class means are within one standard deviation (the average distance from a sample to its class mean) of the other class mean. In this limit, the standard deviations of the classes are both equal to the difference of the class means. For simplicity, the standard deviations of the example distributions depicted in Figure 5(a) and (c) are also equal; however, it is important to note that this is not required when the separation of the distributions is not at the threshold. The relationship between the class means and standard deviations for the threshold of separation is shown in Equation 2:

$$\frac{|\mu_1 - \mu_2|}{\sigma_1 + \sigma_2} = \frac{1}{2}\frac{|\mu_1 - \mu_2|}{\sigma_{1,2}} \geq \frac{1}{2}$$
$$\therefore \frac{(\mu_1 - \mu_2)^2}{(\sigma_1 + \sigma_2)^2} = s_D \geq \frac{1}{4} \tag{2}$$

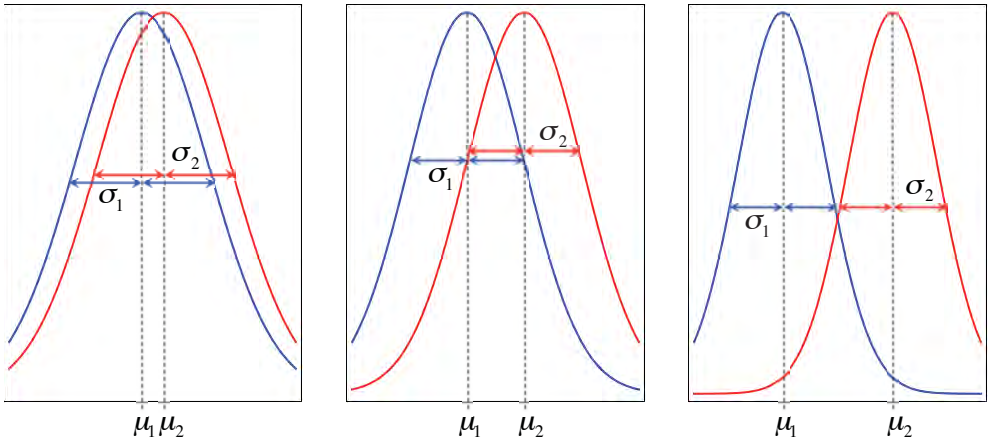

Figure 5: *Binary example of two class distributions with equal standard deviations that are not well separated (a), at the threshold of separation (b), and well separated (c).*

Having a meaningful separation threshold is useful. Currently, the number of features used to form a subset is user-defined; however, if one implemented a threshold for the discriminant score in the feature selection algorithm, it could be used to automatically determine the appropriate number of features to keep.

4.2.3 Principal component analysis

Principal component analysis (PCA) is used to further reduce the dimensionality of the selected features. PCA finds projection directions that are best for maintaining a class-independent overall representation of the data. Initially, there is no reduction in dimensionality as d-dimensional data are projected onto a new d-dimensional space where the projected dimensions are called principal components. The principal components are sorted by variance, a measure of the amount of information about the data they contain. The first principal component is effectively a (multi-dimensional) line of best fit through the data. Additional principal components are orthogonal directions containing monotonically decreasing variance. Most of the variance of the d-dimensional data can be retained by keeping a subset of the top principal components, which therefore reduces the number of dimensions. The number of principal components selected can be determined based on the maximum number of dimensions suggested by the discussion on the curse of dimensionality in Section 4.2.1, by the percentage of total variance to be retained, by maximizing classification performance, or simply by user definition. It is often useful to specify that only 2 principal components be kept to faciliate data visualization.

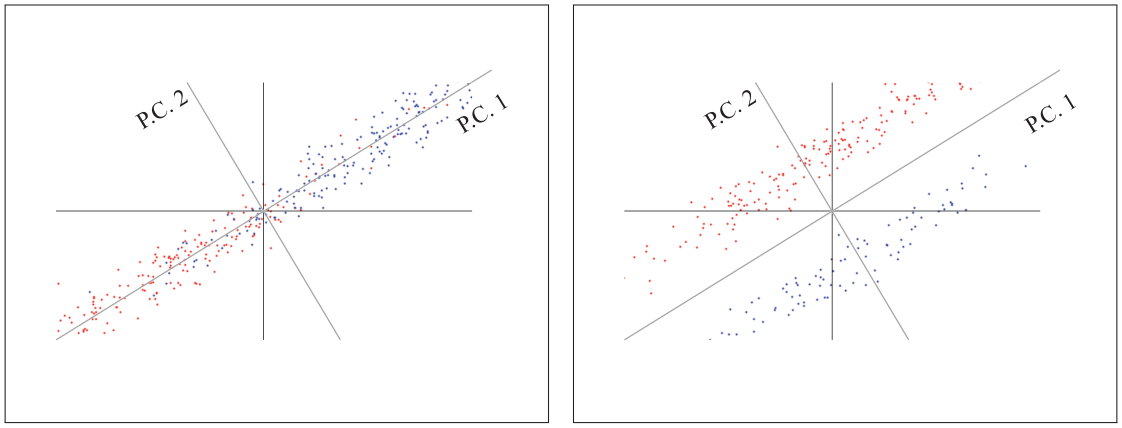

(a) (b)

Figure 6: *Samples from two hypothetical Gaussian distributions with non-zero covariance. The principal components are shown as the diagonal lines labelled P.C. 1 and P.C. 2. In (a), most of the discrimination information is contained in the first principal component. As shown in (b), this is not always the case: the first principal component may not contain any information that allows class separation.*

Figure 6 contains scatter plots of points sampled from two theoretical two-dimensional Gaussian distributions (with non-zero covariance) using a random number generator. The two class distributions are separated by colour. The first principal component is in the direction containing the most variance in the data, and the second principal component is orthogonal to the first. In this example, dimension reduction would involve projecting the

data onto the first principal component axis and discarding the second principal component. It should be noted that PCA does not take class information into consideration. This is demonstrated in Figure 6(b) where the second principal component, the only one that allows class discrimination, would be discarded because it contains less overall variance than the first principal component.

4.3 Gaussian-based classifier

After the aural features are calculated and reduced with feature selection and PCA, a Gaussian-based classifier is applied in which a Gaussian pdf is fit to each class in the training dataset. Although the distributions of the features, and therefore the principal components, are assumed to follow a Gaussian distribution as in [3], this is not typically tested for each dataset, and it is accepted that even if the data do not strictly follow a Gaussian distribution, a simple, successful classification decision boundary can be computed.

The default operating point of the classifier is chosen according to Bayesian decision theory and corresponds to the *Bayes rate* [7] or *minimum-error-rate* [8]. At this operating point, echoes are classified to the more probable class – the class with the higher posterior probability. The posterior probabilities are represented by $P(T \mid \mathbf{x})$ and $P(C \mid \mathbf{x})$ for the clutter and target classes, respectively, and represent the probability of an echo coming from the target class, T, and the probability of an echo coming from the clutter class, C, given the measurement, $\mathbf{x}$. In the case of equal prior probabilities (equal number of samples in class), the decision boundary formed by this operating point is simply the intersection of the Gaussian pdfs. If the prior probabilities are unequal, the posterior probabilities are weighted, and the decision boundary biases classification toward the class with the larger sample size.

The posterior probabilities for the target and clutter classes are calculated from the target and clutter pdfs, $p(\mathbf{x} \mid T)$ and $p(\mathbf{x} \mid C)$, using Equations 5 and 3:

$$P(T \mid \mathbf{x}) = \frac{P(T) \cdot p(\mathbf{x} \mid T)}{P(C) \cdot p(\mathbf{x} \mid C) + P(T) \cdot p(\mathbf{x} \mid T)} \tag{3}$$

$$P(C \mid \mathbf{x}) = \frac{P(C) \cdot p(\mathbf{x} \mid C)}{P(C) \cdot p(\mathbf{x} \mid C) + P(T) \cdot p(\mathbf{x} \mid T)} \tag{4}$$

where $P(T)$ and $P(C)$ are the prior probabilities of the target and clutter classes, and the common denominator normalizes the posterior probabilities such that:

$$P(T \mid \mathbf{x}) + P(C \mid \mathbf{x}) = 1 \tag{5}$$

Figures 7(b) and (d) show the top views of the surfaces for visualization of the decision boundaries. In this case of equal prior probabilities (same number of target and clutter echoes), the decision regions in (b) and (d) are identical, although they may appear slightly different due to the visualization view points.

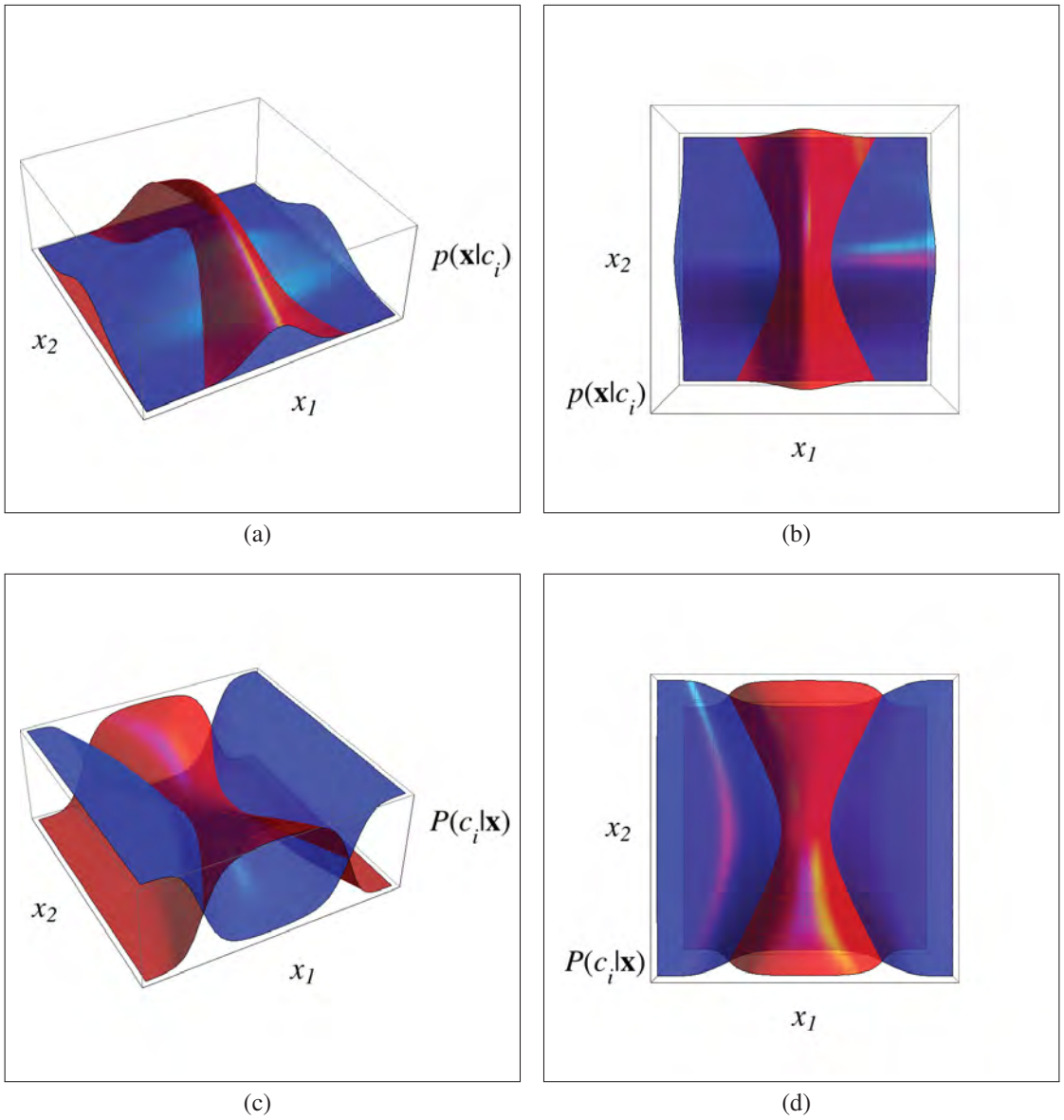

Figure 7: *Hypothetical clutter (blue) and target (red) pdfs shown in (a) and (b), and corresponding posterior probabilities shown in (c) and (d).*

4.4 Classification performance metrics

The simplest measure of performance is classification accuracy, which is defined as the percentage of echoes correctly classified. Individual class accuracies should be calculated, since this information is lost in a total accuracy value. In the multi-class case, accuracy is the only performance metric available; however, in the binary-class case presented in this paper, the receiver-operating-characteristic (ROC) curve, which plots probability of detection versus probability of false alarm, provides more insight on classifier performance.

The default minimum-error-rate operating point specified in Section 4.3 was chosen according to Bayes decision theory, and depending on the relative cost of misclassifying targets and clutter for a given application, this operating point may not be preferred. ROC curves provide a means of quickly evaluating how the classifier is performing at *all* operating points.

A scalar measure of this overall performance is obtained by integrating the area under the ROC curve, A_{ROC}. The ideal ROC curve has a probability of detection of 1 at all false alarm rates (from 0–1), so $A_{\mathrm{ROC}} = 1$ for perfect classification. Theoretically, if classification is performed by random guessing, $A_{\mathrm{ROC}} = 0.5$. $A_{\mathrm{ROC}} > 0.9$ was considered to indicate very successful performance in previous studies on classification of active sonar echoes [2], and this convention is adopted here.

5 Classification results

Recall that the temporal robustness of the aural classifier will be evaluated by training the classifier using data from Clutter07 and testing the classifier using data from Clutter09.

5.1 Training the classifier with Clutter07 data

The first step in training the aural classifier with the Clutter07 echoes is selecting a subset of the large number of echoes available. Two problems can arise from blindly using all of the Clutter07 echoes listed in Table 1. First, there are typically more clutter echoes than target echoes in active sonar. In the Clutter07 dataset there are 39 429 clutter echoes and 19 152 target echoes. Ideally, an equal number of targets and clutter are used so that classification decisions are not biased on prior probabilities calculated from the relative number of target and clutter echoes. Second, the target echoes from both Clutter07 and Clutter09 experiments typically have higher SNR than clutter echoes. The method for calculating SNR used in this study is described in Annex D. Off-beam echoes were extracted, as discussed in Section 3.3, to obtain target echoes with lower SNRs typical of the clutter echoes. To ensure that SNR does not bias classification, the distributions of target and clutter SNRs are matched. The algorithm for matching SNR distributions is very simple. Histograms of the SNR values for each class are first calculated using the same binning for both target and clutter SNR values. The counts in each bin are then matched to within 20% by randomly removing echoes in the bin from the distribution having the higher count. The matched distributions are shown in Figure 8. Note that matching the SNR distributions also solves the first problem by ensuring that there is roughly the same number of target and clutter echoes. After SNR matching, there are 13 133 clutter echoes and 12 366 target echoes.

Table 1: *Identified echoes from Clutter07.*

Underwater object	Number of echoes
Oil rig	118
Wellhead	115
Oil rig off beam	9 555
Wellhead off beam	9 364
Clutter	39 429

The 58 feature values are calculated for each of the target and clutter echoes, 51 of which are found to be non-redundant (not highly correlated over the training dataset). The top five features ranked by discriminant score are selected. The discriminant score ranking method is chosen instead of the overlap fraction method based on the potential advantages discussed in Section 4.2.2. From the top five ranked features, two principal components

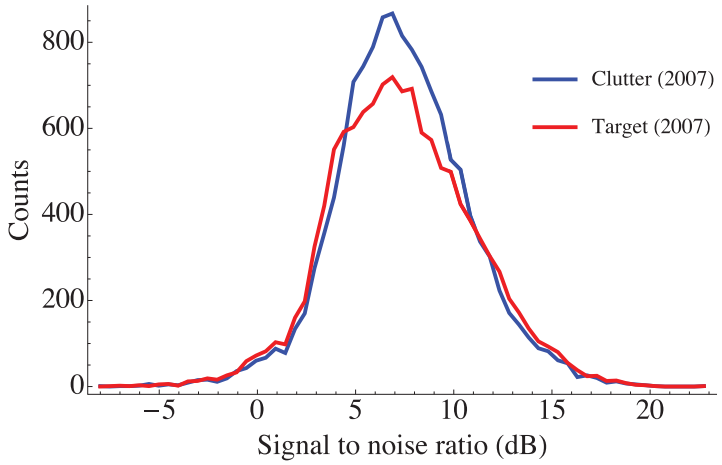

Figure 8: *Histogram of Clutter07 target and clutter SNRs used for training the classifier.*

are kept. The principal components are shown in Table 2 and represent unit vectors that describe the two orthonormal axes onto which the five-dimensional features are projected.

A scatter plot of the principal components for the Clutter07 echoes is shown in Figure 9, where the small blue dots represent clutter echoes and the larger red dots represent target echoes. Since the full dataset of 25 499 points overwhelms a single plot, a representative sample is plotted by taking a random sample of 50 echoes from each class. A decision boundary is calculated by assuming that the class distributions are Gaussian with the observed means and variances. The boundary is plotted as the black circle in Figure 9. Light blue represents the clutter decision region and light red represents the target decision region.

Table 2: *Features and principal components selected during training.*

Feature name	P.C. 1	P.C. 2
peak loudness value	0.4971	0.0178
pre-attack noise peak loudness value	0.4876	-0.0935
loudness centroid	0.3033	0.9165
pre-attack noise integrated loudness	0.4603	-0.3440
psychoacoustic bin-to-bin difference	0.4595	-0.1806

Since the data are not completely separable using the simple decision boundary calculated with the Gaussian classifier, it is useful to *test* the classifier using the same data that was used to *train* it. This provides a baseline for the maximum performance expected since it is not likely that new data will be classified more accurately than that used to train the

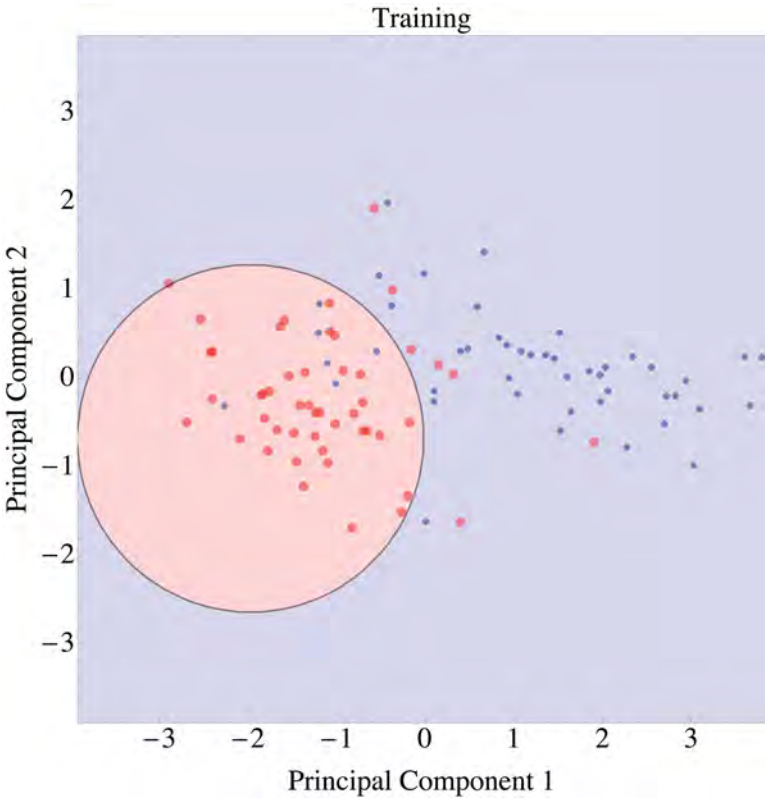

Figure 9: *Scatter plot of training echoes in the reduced two-dimensional feature space. The light red circular target region contains 89% of the target echoes (red points) and the surrounding light blue clutter region contains 77% of the clutter echoes (blue points). Before PCA, the aural feature values are normalized in a class-independent manner such that* $\mu = 0$ *and* $\sigma = 1$ *for all of the echoes in the dataset. Since the principal components plotted are linear combinations of the features, their values have similar statistics – for example, the total mean of all of the echoes is approximately 0 for both principal components.*

classifier. Figure 10 shows the ROC curve generated by testing the classifier with the same Clutter07 data that was used for training. The A_{ROC} value of 0.910 represents the upper limit on performance expected from this classifier when classifying new echo data.

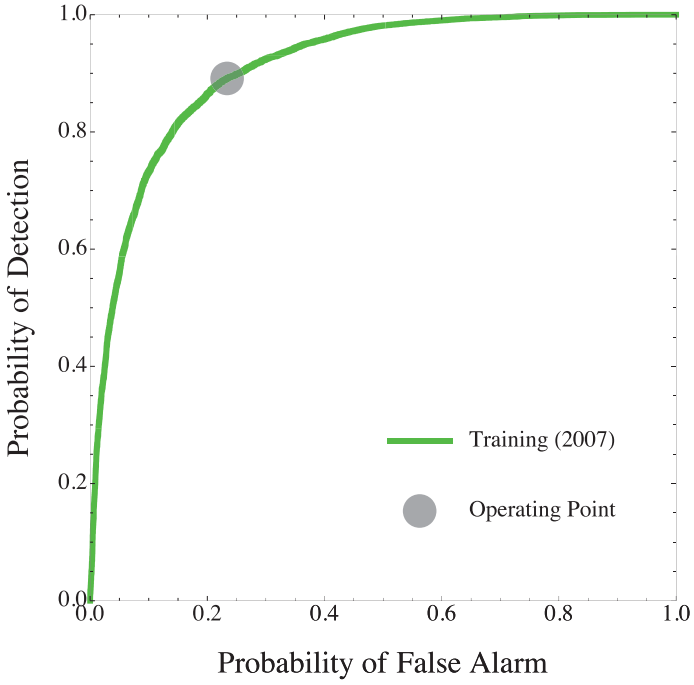

Figure 10: *ROC curve for the Clutter07 training set.*

5.2 Testing the classifier with Clutter09 data

The testing dataset has fewer limitations than the training set; after all, the purpose of a classifier is to classify unidentified echoes. However, for this controlled test in which the identities of the echoes are known, the procedure used on the training dataset to avoid classification biasing is repeated for the testing dataset. In both training and testing phases, it is important to have a similar number of target and clutter echoes when evaluating a classifier using ROC curves. The performance indicated by a ROC curve can be over optimistic when very few targets exist relative to the number of clutter echoes [9], which is typically the case in active sonar.

The original Clutter09 dataset is described in Table 3. It is not necessary to match the target and clutter SNR distributions, but this ensures an equal number of target and clutter echoes, and even in the testing phase, the classification results should not be biased by differences in SNR that may lead to higher discrimination between target and clutter echoes. To be consistent with the training SNRs, the testing SNR distributions are made similar by bin-matching each of the target and clutter SNR distributions to within 20% of their respective training distributions. Since a 20% discrepancy was allowed between bins in the training distributions, a maximum discrepancy of 44% ($1.2^2 = 1.44$) is possible between the testing target and clutter SNR distributions. Allowing some discrepancy avoids discarding too

Table 3: *Identified echoes from Clutter09.*

Underwater object	Number of echoes
Oil rig	124
Wellhead	129
Oil rig off beam	6 345
Wellhead off beam	7 129
Clutter	22 916

many echoes, and retains a relatively large dataset. The matched distributions for the testing set are shown in Figure 11.

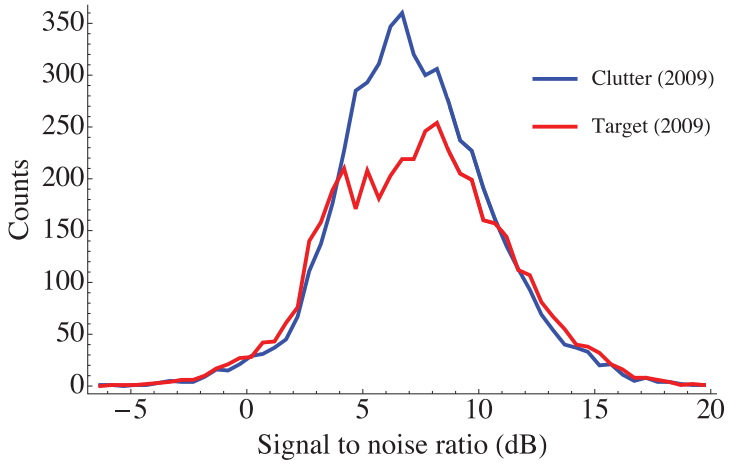

Figure 11: *Histogram of Clutter09 target and clutter SNRs used for testing the classifier.*

After SNR matching, the number of target echoes from Clutter09 is 4,438 and the number of clutter echoes is 5,204. The number of testing echoes is much smaller than the number of training echoes (Section 5.1) because fewer echoes were present in the testing dataset, and matching the SNR distributions to the specific training distributions reduces the dataset more than simply matching the target and clutter distributions.

The decision boundary generated in Section 5.1 represents the trained classifier at the minimum-error-rate operating point. A discussion on operating points can be found in [8]. The testing echoes are converted to two dimensions using the same five features and two principal components (listed in Table 2) that were used to train the classifier. A representative sample of 50 echoes from each class are shown in the scatter plot in Figure 12. The existing decision boundary is used to determine how many targets are classified correctly

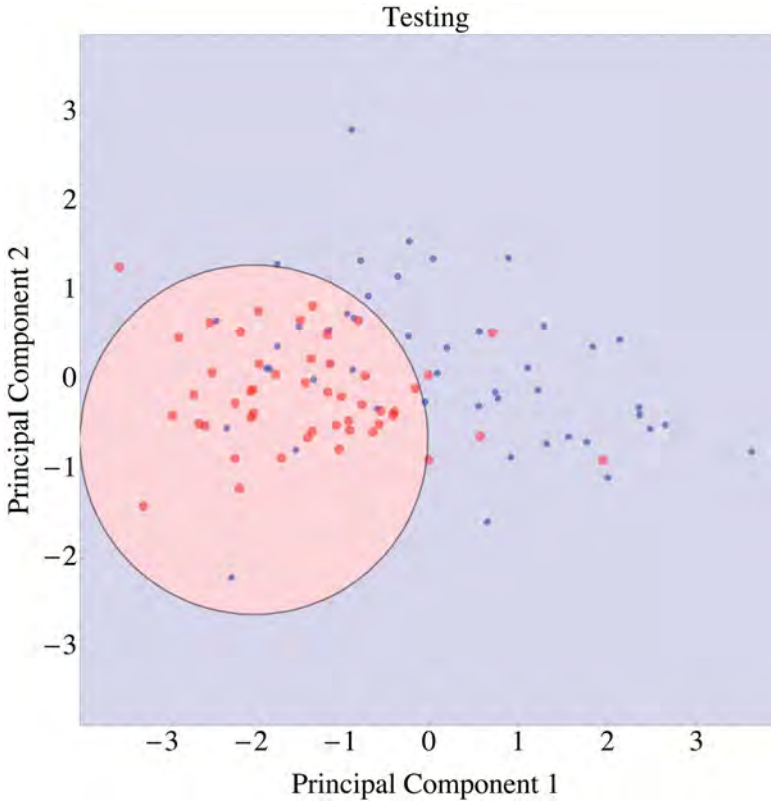

Figure 12: *Scatter plot of testing echoes in the reduced (two-dimensional) feature space. The light red circular target region contains 90% of the target echoes (red points) and the surrounding light blue clutter region contains 64% of the clutter echoes (blue points).*

(large red dots in circular red region) and how many clutter echoes are classified correctly (small blue dots in blue region surrounding the circle).

The ROC curve with $A_{\mathrm{ROC}} = 0.856$ is shown as the dashed orange line in Figure 13, added to the green coloured training ROC curve first shown in Figure 10. The classification performance indicated by A_{ROC} is very promising given the experimental differences between Clutter07 and Clutter09. The performance goal of $A_{\mathrm{ROC}} > 0.9$ is approached, and the next section looks at improving performance to this level.

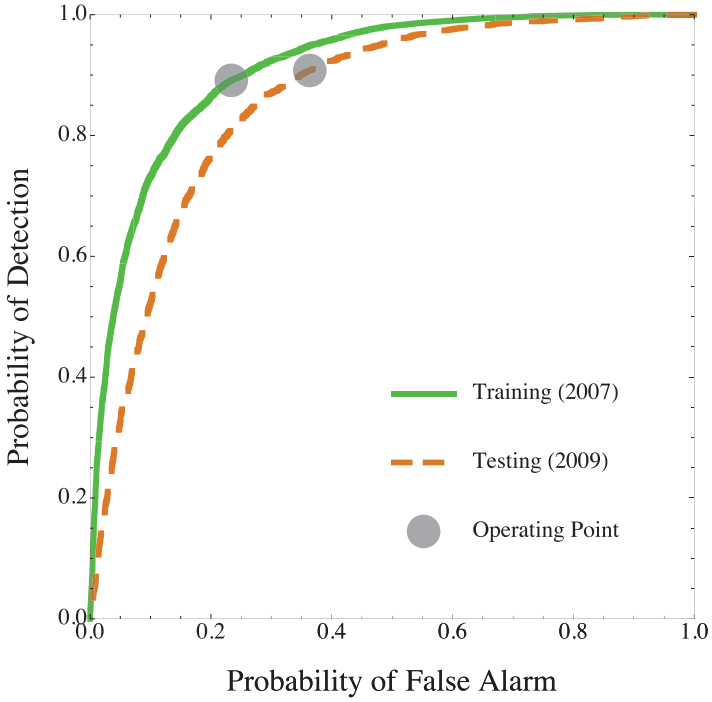

Figure 13: *ROC curve for the Clutter09 testing dataset.*

5.3 Improving the performance of the classifier

The number of features and principal components used to reduce dimensionality are both user-defined parameters. Varying these parameters affects classifier performance, so it is logical to test all possible combinations of the parameters within their common range of 2–51 to see if performance can be increased from that achieved with the original settings (five features, two principal components). Discussion in Section 4.2.1 suggested that the number of dimensions should be less than four for the size of the current datasets. This limitation is not imposed on the number of principal components in searching for maximum performance, but it should be kept in mind.

Since features are chosen in decreasing order of discriminant rank, additional features will provide successively smaller classification improvements; and at some point they may degrade performance since they can potentially act like noise. This is shown in Figure 14 which plots performance (A_{ROC}) as the number of features is increased along the horizontal axis and the number of principal components is increased on the vertical axis. As expected, the performance peaks and then begins to decrease as lower ranked features (i.e., 30–50) are added. Note that the number of principal components cannot exceed the number of features so data only exist below the diagonal. Also, according to the discussion on the

curse of dimensionality in Section 4.2.1, large numbers of principal components should be not used. The training results are shown in Figure 14(a) and the maximum, $A_{\mathrm{ROC}} = \mathbf{0.943}$, occurs at 17 features and 2 principal components. In testing the Clutter09 data shown in Figure 14(b), the maximum, $A_{\mathrm{ROC}} = \mathbf{0.903}$, occurs at 29 features and 3 principal components. Achieving $A_{\mathrm{ROC}} > 0.9$ in the testing case indicates successful classification and therefore temporal robustness, and is the main result presented in this work.

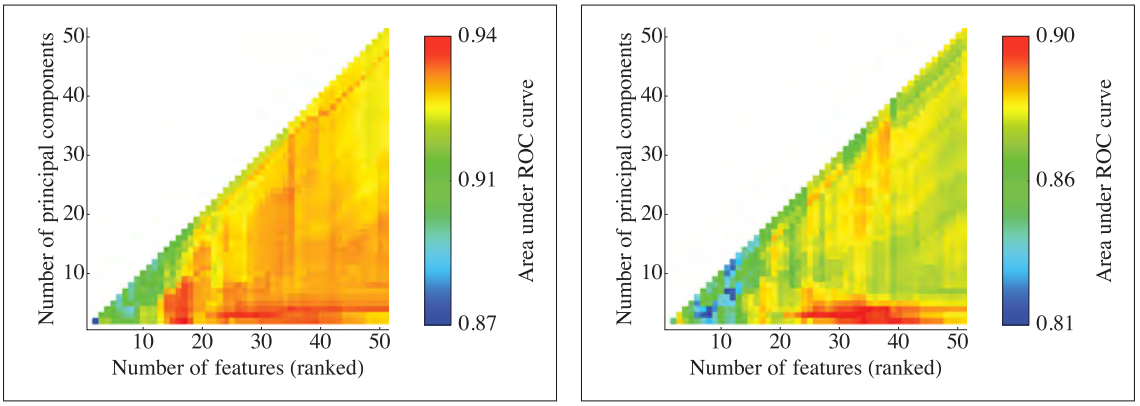

(a) Training (classifier tested using the same Clutter07 dataset used for training) with features ranked by discrimant score. A_{ROC} array max of 0.943 at 17 features, 2 principal components.

(b) Testing (classifier trained with Clutter07 data, tested with Clutter09 data) with features ranked discriminant score, max A_{ROC} of 0.903 at 29 features, 3 principal components.

Figure 14: *Classifier performance as a function of number of features (ranked by discriminant score) and principal components used.*

5.4 Feature selection comparison

In the last three sections, discriminant score was used to rank features; however, the aural classifier achieved successful classification using the overlap fraction method in previous studies [10]. This section evaluates classification performance of the overlap fraction compared to the performance acheived with discriminant score in the last section.

The overlap fraction values and discriminant score values calculated from the training data are ordered and plotted as a series in Figure 15(a). Note that the horizontal axis is the feature rank (in order) and may correspond to a different aural feature for each ranking method. For example, the top ranked feature using discriminant score is the *peak loudness value* and the top feature for the overlap fraction method is the *local minimum sub-band decay slope*. For the full list of features ordered by overlap fraction and discriminant score, see Table E.1.

In order to compare the values used to rank the features with both methods, the values are normalized so that they range from 1 (for highest rank) to 0 (for lowest rank). These values

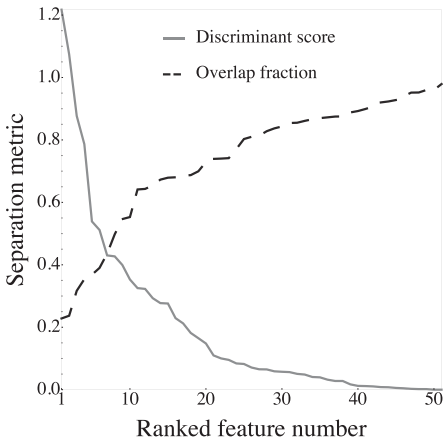

(a) Discriminant scores (solid line) and overlap fractions (dashed line) versus their respective ordered features.

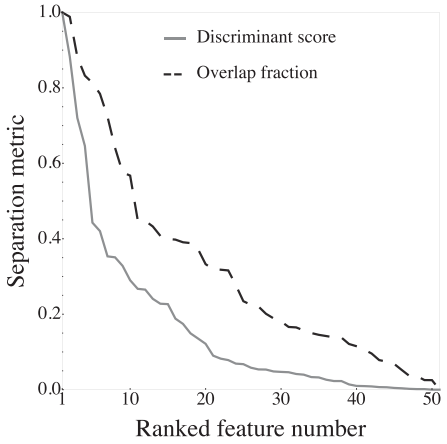

(b) Normalized discriminant scores (solid line) and overlap fractions (dashed line) decreasing with respective ordered feature rank.

Figure 15: *Comparison of discriminant scores to overlap fractions.*

are plotted in Figure 15(b). The discriminant score values decrease rapidly, suggesting that the the higher ranked features are much stronger than the lower ranked features. The overlap fractions decrease in a similar fashion, but do not approach zero as rapidly. This makes the discriminant score method more appealing because there is more definition between the top and bottom ranked features.

To compare performance with that achieved using the discriminant score ranking method, the procedure used to produce Figure 14 with the discriminant score method is repeated with the overlap fraction method. The plots are shown in Figure 16. To facilate direct comparison, the testing cases are plotted side by side with identical color ranges in Figure 17.

The maximum performance achieved with the overlap fraction method ($A_{\mathrm{ROC}} = 0.941$ for training and $A_{\mathrm{ROC}} = 0.904$ for testing) is similar to that of the discriminant score method, so there is no gain in maximum performance by switching ranking methods from overlap fraction to discriminant score. However, it is important to note that the minimum of the training and testing performances (indicated by the lower limit A_{ROC} values printed on the color scales in Figures 14 and 16) are *lower* for the overlap fraction method. Furthermore, at lower numbers of features (< 5), the discriminant score method outperforms the overlap fraction (Figure 17), indicating that the top features ranked by discriminant score are better for classification. In addition, more features (38 compared to 29) are required for the overlap fraction to reach the maximum testing performance of the discriminant score method. Although the discriminant score method does not provide a strong advantage for the datasets presented, evidence in Figures 15 and 16 suggests that it is the preferred method of ranking features.

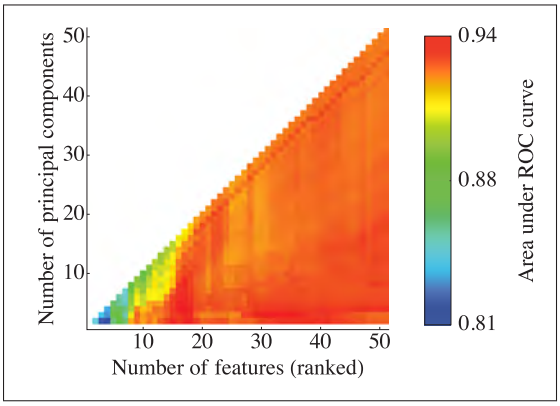

(a) Training (classifier tested using the same Clutter07 dataset used for training) with features ranked by overlap fraction, max A_{ROC} of 0.941 at 17 features, 4 principal components.

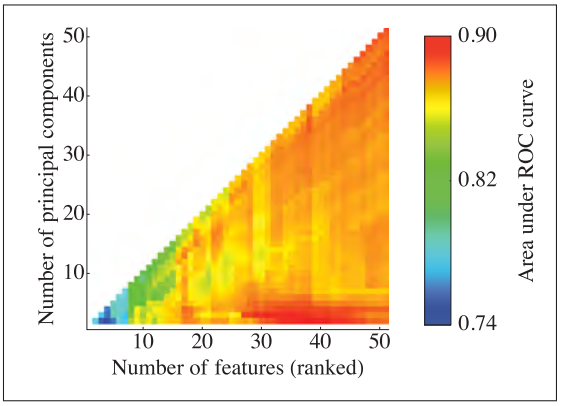

(b) Testing (classifier trained with Clutter07 data, tested with Clutter09 data) with features ranked by overlap fraction, max A_{ROC} of 0.904 at 38 features, 2 principal components.

Figure 16: *Classifier performance as a function of the number of features (ranked by overlap fraction) and principal components used.*

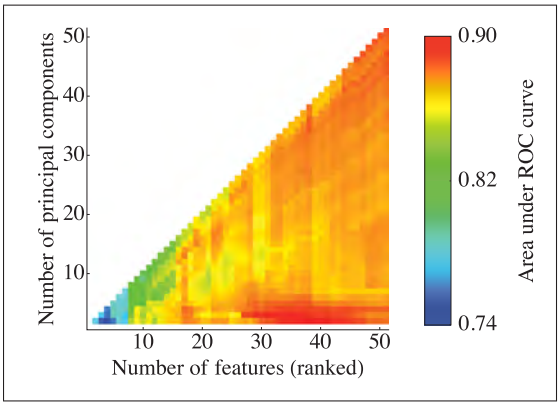

(a) Testing with overlap fraction, max A_{ROC} of 0.904 at 38 features, 2 principal components.

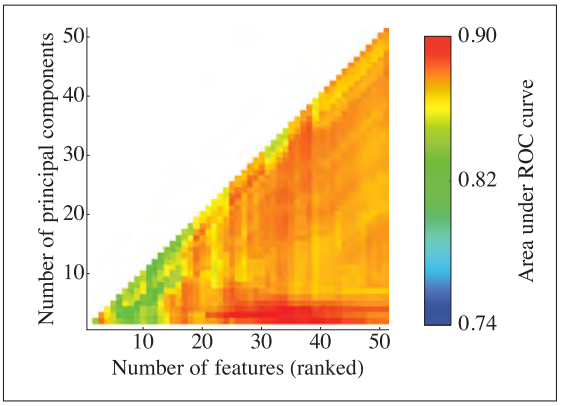

(b) Testing with discriminant score, max A_{ROC} of 0.903 at 29 features, 3 principal components.

Figure 17: *Classifier testing performance for the overlap fraction (a) and discriminant score (b) feature ranking methods. The color ranges are identical to allow direct comparison.*

6 Conclusions and future work

This paper examined the temporal robustness of DRDC's aural classifier. The aural classifier mimics the human auditory system in order to automate the capability of sonar operators to distinguish clutter from targets. Binary classification of Clutter09 echoes as either targets or clutter was performed after training the classifier with older data from a previous sea trial, Clutter07. Successful classification was indicated by achieving an area under the ROC curve of $A_{\mathrm{ROC}} = 0.903$, recalling that $A_{\mathrm{ROC}} = 1$ for perfect classification and $A_{\mathrm{ROC}} = 0.5$ for random guessing. This is a very promising result in light of the different sound propagation conditions between experiments.

The aural classifier has high potential for implementation in military active sonar systems, since it can be trained in advance and used for long-term classification of echoes over a range of environmental conditions. Operational sonar systems frequently mistake clutter for targets in coastal waters, resulting in high false alarm rates. By providing false alarm reduction, the aural classifier could greatly improve detection performance of these systems, and also reduce operator load.

Future work will involve expanding the database to include data from additional experiments in Clutter09. The dependence of classification on SNR will also be examined to study the difficult case of classifying low SNR echoes. Finally, true discriminant analysis will be implemented and tested, which will accomplish dimension reduction by projecting the aural features onto axes that maximize discrimation between targets and clutter. This will be compared to the feature selection method and principal component analysis technique currently used to reduce dimensionality.

References

[1] Allen, N. (2008), Receiver-operating-characteristic (ROC) analysis applied to listening-test data: Measures of performance in aural classification of sonar echoes, (DRDC Atlantic TM 2007-353) Defence R&D Canada – Atlantic.

[2] Hines, P. C., Allen, N., and Young, V. W. (2008), Aural classification for active sonar: Final Report for TIF Project 11CQ11 "Aural Discrimination of True Targets from Geological Clutter", (DRDC Atlantic TM 2007-361) Defence R&D Canada – Atlantic.

[3] Young, V. W. and Hines, P. C. (2007), Perception-based automatic classification of impulsive-source active sonar echoes, *J. Acoust. Soc. Am.*, 122(3), 1502–1517.

[4] Urick, R. J. (1975), Principles of underwater sound, 2nd ed, McGraw-Hill, Inc.

[5] Abraham, D. A. and Willett, P. K. (2002), Active sonar detection in shallow water using the Page test, *IEEE Journal of Oceanic Engineering*, 27(1), 35–46.

[6] Hood, J. and McInnis, J. (2010), Integrated tracker and aural classifier (ITAC) development, (DRDC Atlantic CR 2010-049) Akoostix Inc.

[7] Hastie, T., Tibshirani, R., and Friedman, J. (2001), The elements of statistical learning; data mining, inference, and prediction, New York: Springer.

[8] Duda, R. O., Hart, P. E., and Stork, D. G. (2001), Pattern Classification, 2nd ed, Wiley-Interscience.

[9] Davis, J. and Goadrich, M. (2006), The relationship between precision-recall and ROC curves, In *Proceedings of the 23rd International Conference on Machine Learning*, Pittsburgh, PA.

[10] Hines, P. C., Young, V. W., and Scrutton, J. (2008), Aural classification of coherent-source active sonar echoes, In *Proceedings: International Symposium on Underwater Reverberation and Clutter*, Lerici, Italy.

Annex A: Ship waypoints

Tables A.1 and A.2 list the time-stamped ship waypoints for the tracks followed by NRV ALLIANCE during the Clutter07 and Clutter09 sea trials.

Ping times between the start and end of turns are omitted in this work due to large bearing error in contact location.

Table A.1: *Ship track waypoints during experiment in Clutter07.*

Waypoint #	Waypoint name	Time (UTC)	Latitude (° N)	Longitude (° E)
1	*Start of track*	0805	36.581803	14.563557
2	*Start of turn 1*	0922	36.495507	14.563417
3	*End of turn 1*	0938	36.487869	14.581897
4	*Start of turn 2*	1010	36.488953	14.627526
5	*End of turn 2*	1030	36.473951	14.642554
6	*Start of turn 3*	1310	36.296002	14.688598
7	*End of turn 3*	1334	36.285475	14.713652
8	*End of track*	1604	36.287636	14.920981

Table A.2: *Ship track waypoints during experiment in Clutter09.*

Waypoint #	Waypoint name	Time (UTC)	Latitude (° N)	Longitude (° E)
1	*Start of track*	0913	36.579939	14.563641
2	*Start of turn 1*	1003	36.509475	14.563333
3	*End of turn 1*	1030	36.489167	14.595960
4	*Start of turn 2*	1040	36.489167	14.613313
5	*End of turn 2*	1104	36.471409	14.641495
6	*Start of turn 3*	1310	36.300606	14.687429
7	*End of turn 3*	1330	36.287833	14.714066
8	*End of track*	1540	36.287833	14.933773

This page intentionally left blank.

Annex B: Experimental details

Tables B.1 lists some miscellaneous experimental details for Clutter07 and Clutter09.

Table B.1: *Experimental details for Clutter07 and Clutter09.*

Property	Value
Date of Clutter07 experiment	May 29, 2007 (calendar day 149)
Date of Clutter09 experiment	May 3, 2009 (calendar day 123)
Clutter07 average true wind speed	15.2 knots @175.7° rel. true N
Clutter09 average true wind speed	3.8 knots @92.9° rel. true N
Number of hydrophone (triplets) in cardioid array	85
Cardioid array hydrophone spacing	21 cm
Nominal upper operating frequency of cardioid array	3620 Hz
Data acquisition rate from hydrophones	12.8 kHz
Number of beams formed	120
Beam spacing	Equally spaced in cosine of beam angle
Heterodyning frequency	1950 Hz
Data decimation factor	3
Sampling rate after heterodyning	4.2667 kHz
Campo Vega oil rig coordinates	36.539033° N, 14.625400° E
Campo Vega wellhead coordinates	36.558887° N, 14.637217° E
Malta Plateau local magnetic declination	2.5°

This page intentionally left blank.

Annex C: Reverberation statistics

C.1 Detection

When an active sonar ping is transmitted underwater, the receiver measures reverberation even if echoes from strong reflectors – manmade or geological – are absent. If it is assumed that this reverberation is caused by the sum of contributions from many scatterers, then the instantaneous amplitude of the reverberation signal should have Gaussian statistics according to the Central Limit Theorem. The envelope of the reverberation therefore follows a Rayleigh distribution, and the intensity (squared envelope) follows an exponential distribution. Reverberation statistics are discussed in further detail in the next section (C.2), where the assumption that Clutter09 reverberation intensity data is distributed exponentially is also validated.

If the reverberation is stationary (constant average power) and the reverberation intensity is assumed to follow an exponential distribution, a false alarm rate can be specified, where from the detector standpoint, a false alarm indicates a detection caused by reverberation in the absence of a legitimate echo return (contact). However, since the reverberation power is not constant but rather decays with time, normalization of receiver data is required. As depicted in Figure C.1, the (enveloped, matched-filtered) receiver time series data are normalized using a split-window normalizer that estimates reverberation and background noise power from samples of auxiliary data adjacent (separated by guard bands) to the sample being normalized. Samples in the normalized data that exceed a specified threshold (set by the false alarm rate requirement) are considered to be detections [5].

An automatic detector that uses split-window normalization was developed for Clutter09 by the author of [5]. Assuming exponentially distributed reverberation intensity data, a probability of false alarm (PFA) of 1.0×10^{-6} was specified and used to determine a signal-to-noise ratio (SNR) threshold of 13.82 (11.40 dB) using Equation C.8 which is introduced later in this section. In normalizing the enveloped, matched-filtered time series with the split-window method, the SNR of each sample is calculated, since each sample (instantaneous power) is divided by an estimate of surrounding noise power. The matched-filter employed by the detector uses a parameter-generated replica of an LFM from 500–3500 Hz with a duration of 1.1 s, shaded using a raised cosine taper for the first and last 100 Hz of the LFM.

Ideally, each echo is associated with a single detection; however, a single event, or echo, can contain many raw detections, therefore a method of refining or clustering the detections is required. *Time clustering* and *beam clustering* are performed to refine detections over range and across bearing.

The detector starts by refining each beam time series individually (time clustering). For each beam, the detection with the largest amplitude is isolated, and any other detections

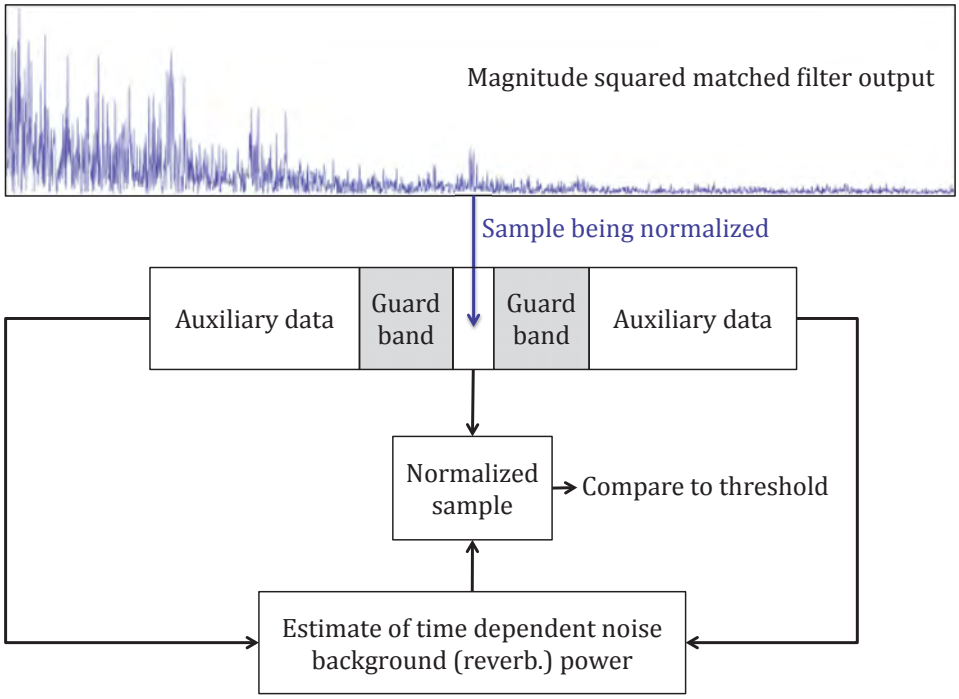

Figure C.1: *Split-window normalizer used by the detector. Figure reconstructed from [5].*

within 50 ms are considered to be associated. These detections are removed. This is repeated for the next highest detection, and so on, so that each detection is separated from other detections by at least 50 ms. Note that echoes with durations longer than 50 ms can contain multiple refined detections.

Next, the detections are clustered across beams, to remove instances of echoes on multiple beams caused by signal leakage into sidelobes. The assumed contact beam is the one with the highest SNR detection, and instances of the detection on other beams are removed from the detection list. Similar to time clustering, beam clustering starts with the highest SNR (time-clustered) detection. Detections occurring within 10 ms on different beams are candidates for association. For detections with SNR $<$ 20 dB, any candidate detections within 6 beams are associated. Detections with 20–25 dB SNR have candidate detections within 8 beams associated, and for detections with SNR $>$ 25 dB, candidate detections on all beams are associated. As with time clustering, all associations are removed from the list of detections, associations are determined for the next highest detection, and so on.

The cardioid left-right ambiguity suppression in NURC's beamformer also has limitations, so high SNR echoes may be observed on ambiguous beams. An ambiguous beam has the same angle from end-fire as the contact beam, only it is on the opposite side of the array. If a detection's SNR $>$ 18 dB, candidate detections on beams ambiguous with those considered (according to SNR) in the last paragraph are also associated.

Even with a low detection PFA with time and beam clustering, the number of detections per ping is large when strong scatterers (clutter) are present. The detections used in this work are based on a constant threshold (11.40 dB), however, an adaptive threshold detector ran in parallel and typically reported fewer detections. Although the adaptive threshold detections are not considered here, the number of constant threshold detections was reduced to the number of adaptive threshold detections by removing the lowest SNR constant threshold detections.

This section on detection ends with a short discussion on SNR. It is important to note that the SNR calculation performed by the detector is different than that described in Appendix D and used throughout the rest of the paper. The difference lies in the measure of the signal power used to calculate the ratio. The SNR calculation for each detection by the detector compares the *instantaneous* amplitude of the detection sample with an average of the surrounding noise power to compute a ratio. During the clustering process, a number of detections are reduced to a single detection which retains the *maximum* SNR of the detections in the cluster. This value is always greater than the near-peak *average* calculated in Appendix D, since values surrounding the maximum used to compute the average are inherently lower. This explains why the echo SNRs shown in Section 5 can have values below the 11.40 dB threshold implemented by the detector in this section.

C.2 Statistics theory applied to generated noise

The detector described in Section C.1 uses the assumption that reverberation follows a Gaussian distribution, and therefore that reverberation intensity is distributed exponentially. This section reviews the statistics theory that relates the Gaussian distribution to the Rayleigh and exponential distributions. A computer generated noise time series is used to provide signal visualization and to demonstrate some implications of the statistics theory. A sample of beamformed, matched-filtered time series data from Clutter09 is then analyzed in Section C.3 to validate the reverberation statistics that were assumed in developing the detector.

C.2.1 Gaussian distributed noise

Figure C.2(a) shows 2^{16} samples of a discrete noise signal, $g[n]$, produced with a random number generator sampling from a standard Gaussian probability density function (pdf):

$$f\left(x;\,\mu,\sigma^2\right) = \frac{1}{\sqrt{2\pi\sigma^2}} e^{-\frac{(x-\mu)^2}{2\sigma^2}} \quad \text{(Gaussian pdf)} \tag{C.1}$$

where μ is the mean and σ^2 is the variance. For the standard Gaussian distribution, $\mu = 0$ and $\sigma^2 = 1$, and this pdf is plotted as the gray dashed line in Figure C.2(b). The probability

mass function (pmf) of the discrete noise signal is plotted in black and, by design, matches the pdf from which it was randomly sampled. Recall that the pmf is used for discrete random variables and the pdf is used for continous random variables. Here, the pmf is calculated by taking a histogram of the signal and scaling the bin counts so that the area under the histogram is normalized to 1.

A random variable X that is Gaussian distributed is denoted by $X \sim \mathcal{G}\left(\mu, \sigma^2\right)$.

C.2.2 Rayleigh distributed envelope

The Rayleigh pdf is given by Equation C.2:

$$f(x;\, \sigma) = \frac{x}{\sigma^2} e^{-\frac{x^2}{2\sigma^2}},\ x \geq 0 \quad \text{(Rayleigh pdf)} \tag{C.2}$$

If $X \sim \mathcal{G}\left(0, \sigma^2\right)$ and $Y \sim \mathcal{G}\left(0, \sigma^2\right)$ are two statistically independent variables with Gaussian distributions, and a random variable R is calculated as $R = \sqrt{X^2 + Y^2}$, then R is Rayleigh distributed: $R \sim \text{Rayleigh}(\sigma)$. The envelope of a signal is calculated by taking the magnitude of its analytic (complex) signal. The following details of the envelope calculation show that the envelope of noise generated with the random variable $X \sim \mathcal{G}\left(\mu, \sigma^2\right)$ is equivalent to $\sqrt{X^2 + Y^2}$, and therefore follows a Rayleigh distribution.

First, the analytic signal, $x_a(t)$, is defined as:

$$x_a(t) = x(t) + j\hat{x}(t) \tag{C.3}$$

where $\hat{x}(t)$ is the *Hilbert transform* of $x(t)$, and has a quadrature phase relationship (90° phase shift) with $x(t)$. The magnitude, or envelope, of $x(t)$ is then calculated as:

$$|x_a(t)| = \sqrt{x^2(t) + \hat{x}^2(t)} \tag{C.4}$$

The in-phase $[x(t)]$ and quadrature $[\hat{x}(t)]$ components are statistically independent and identically Gaussian distributed, so it follows that the square-root of the sum of their squares (the envelope) is Rayleigh distributed. The example noise envelope, $|g_a[n]| = \sqrt{g^2[n] + \hat{g}^2[n]}$, is shown in Figure C.3. The theoretical Rayleigh pdf, $f(x;\, \sigma) = f(x;\, 1) = xe^{-x^2/2}$ is shown and closely matches the pmf of $|g_a[n]|$.

C.2.3 Exponentially distributed intensity

Intensity is proportional to amplitude squared, therefore squaring the envelope signal results in an intensity signal. If R is a Rayleigh distributed random variable, or $R \sim \text{Rayleigh}(\sigma)$, then $R^2 \sim \text{Exponential}\left(1/2\sigma^2\right)$. The exponential pdf is given by:

$$f(x;\, \lambda) = \lambda e^{-\lambda x},\ x \geq 0 \quad \text{(Exponential pdf)} \tag{C.5}$$

where λ is known as the rate parameter.

The intensity signal, $|g_a[n]|^2$, is shown in Figure C.4. The pmf of the intensity signal closely matches the expected exponential pdf, $f\left(x;\, 1/2\sigma^2\right) = f(x;\, 1/2) = 0.5e^{-0.5x}$.

When the intensity is normalized with the split-window normalizer (Section C.1), the resulting signal, shown in Figure C.5(a), represents instantaneous SNR. Figure C.5(b) compares the signal pmf and the theoretical standard exponential distribution: $f(x;\, 1) = e^{-x}$. The expected value of the standard exponential distribution is $E[X] = \lambda^{-1} = 1$. This expected value of SNR is logical: the noise is stationary (constant average power or intensity), so in the absence of signal, the intensity of any noise sample is expected to be equal to the average intensity of the rest of the noise samples (i.e., a ratio of 1).

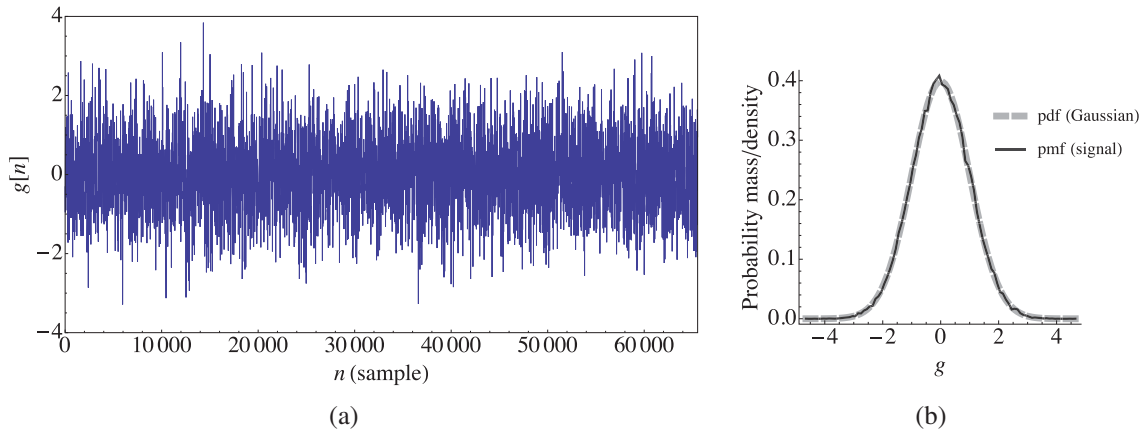

(a) (b)

Figure C.2: *Noise signal, $g[n]$, shown in (a) generated by randomly sampling the Gaussian pdf shown as the dashed line in (b). The pmf of the generated signal is also shown in (b).*

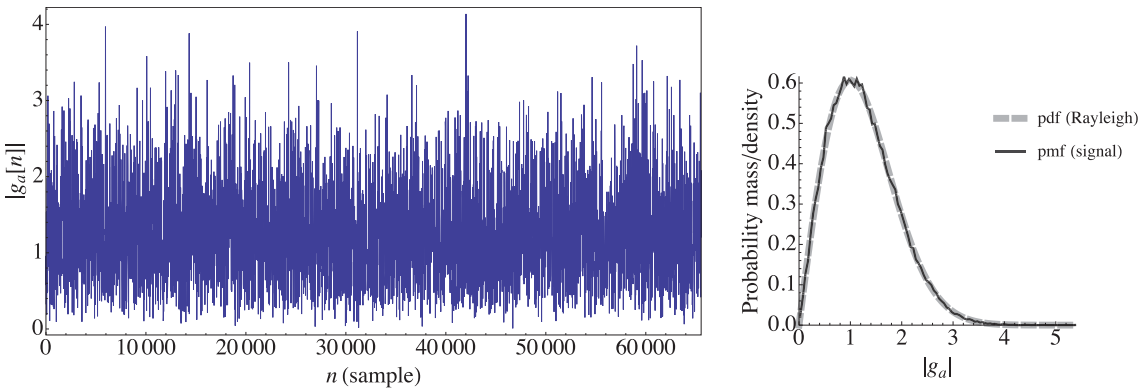

(a) (b)

Figure C.3: *Enveloped noise signal, $|g_a[n]|$, shown in (a) and its pmf in (b). The theoretical Rayleigh pdf is also shown in (b).*

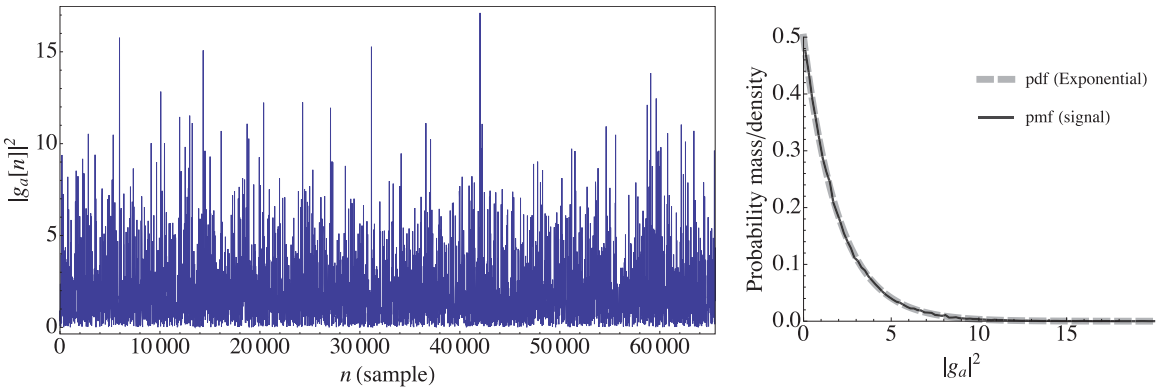

Figure C.4: *Squared noise envelope signal (intensity), $|g_a[n]|^2$, shown in (a) and its pmf in (b). The theoretical exponential pdf is also shown in (b).*

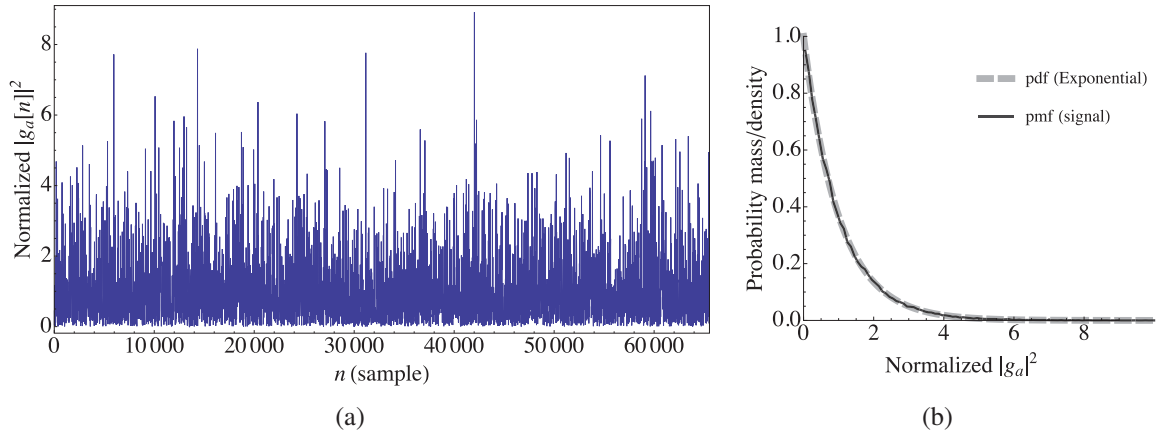

Figure C.5: *Squared noise envelope signal (intensity) normalized with the split-window normalizer shown in (a) and its pmf in (b). The theoretical standard exponential pdf is also shown in (b).*

For detection applications, the probability measure of interest is not the probability density discussed in this section, but rather the probability of false alarm (PFA). The PFA is the probability that a random sample X has a value (SNR) greater than a detection threshold, x_{det}: $P(X \geq x_{det})$. If SNR is standard exponential distributed, this probability can be calculated by taking the integral of the standard exponential pdf over the interval (x_{det}, ∞):

$$\begin{aligned} \text{PFA} = P(X \geq x_{det}) &= \int_{x_{det}}^{\infty} e^{-x}\, dx \qquad \text{(C.6)} \\ &= -e^{-x}\Big|_{x_{det}}^{\infty} \\ &= (0) - \left(-e^{-x_{det}}\right) \\ \text{PFA} &= e^{-x_{det}} \qquad \text{(C.7)} \end{aligned}$$

In order to calculate the detection threshold for a given PFA, Equation C.7 is solved for x_{det}:

$$x_{det} = -\ln(\text{PFA}) \qquad \text{(C.8)}$$

C.3 Clutter09 reverberation

The previous example used stationary noise – noise with constant average power over the duration of the signal. In active sonar, reverberation is not stationary, rather it decays with time because echoes arriving at later times are returned from scatterers at longer ranges, and therefore undergo greater transmission loss.

Figure C.6(a) shows an example of a matched-filtered time series (on the aft end-fire beam), $z[n]$, recorded following transmission of an LFM during the Clutter09 sea trial. The direct blast is observed at the start of the signal, and reverberation decay is noticable over the first 100 000 samples. The spikes seen at approximately 220 000 and 240 000 samples are caused by echoes returned from Campo Vega's oil rig and wellhead, respectively. The pmf of the signal is shown in Figure C.6(b), and the signal's mean and variance are used to generate the theoretical Gaussian pdf, also plotted in the figure.

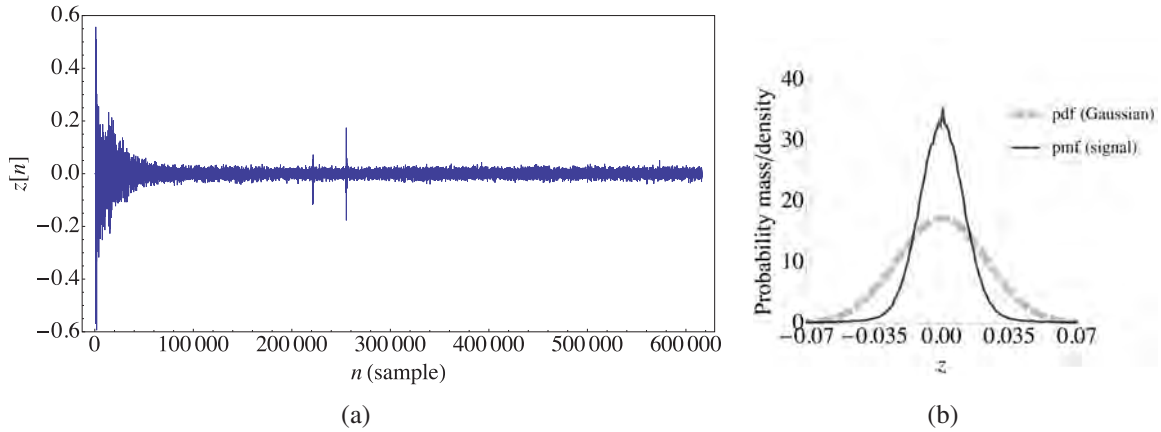

Figure C.6: *Matched-filtered time series data for a single beam recorded during the Clutter09 sea trial shown in (a), and its pmf in (b). The theoretical Gaussian pdf is also shown in (b).*

The pmf of the un-normalized total signal from Clutter09 does not match the Gaussian pdf generated with the mean and standard deviation of the signal, $\mu = 1.10 \times 10^{-7}$, and $\sigma = 0.0230$. This is not surprising because the total signal is clearly not stationary due to the reverberation decay noticable over the first 100 000 samples.

Analyzing the distribution of samples 100 0000–600 000 that appear to be stationary helps to clarify why the signal pmf deviates from the Gaussian pdf with the same statistics. These samples are plotted along with the pmf and Gaussian pdf in Figure C.7. When only the samples beyond the first 100 000 are considered, the signal pmf closely matches the Gaussian pdf generated with the signal's statistics, $\mu = 1.65 \times 10^{-7}$, and $\sigma = 0.0118$. The pmf of this partial signal is also very similar to the pmf of the total signal that was shown in Figure C.6. The first 100 000 samples compose only one sixth of the overall signal, and

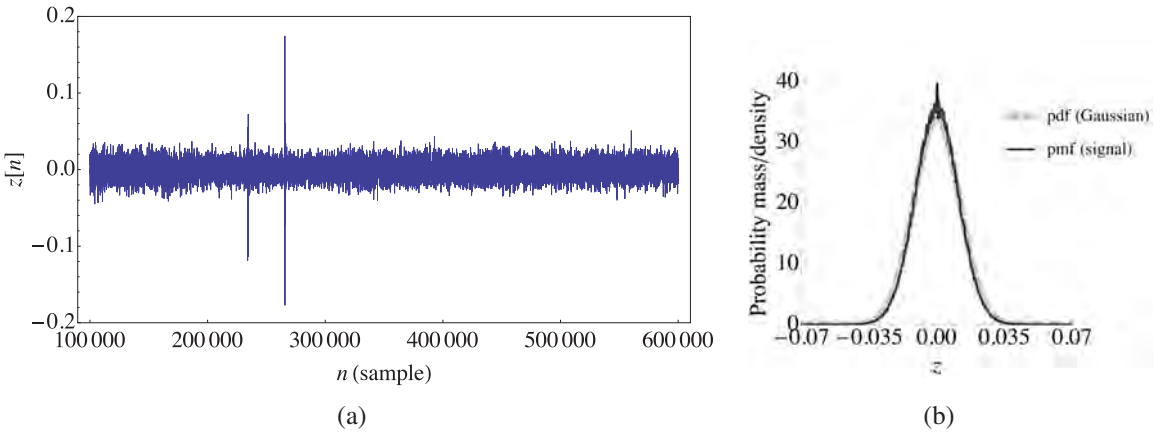

Figure C.7: *Samples 100 000–600 000 of the data shown in Figure C.6 are displayed in (a), and its pmf in (b). The theoretical Gaussian pdf is also shown in (b).*

evidently do not have a significant influence on the total signal pmf. However, the larger amplitudes present in the first 100 000 samples nearly double the total variance to 0.0230 from the value of 0.0118 measured in the last 500 000 samples. This explains why the Gaussian pdf generated with the statistics of the total signal had a larger spread than the pmf measured: the large variance contributed to the total signal by the first sixth of the signal (used to generate the Gaussian pdf) was not evident in the distribution of the total signal driven by the majority (five sixths) of the data that had lower variance.

The split-window normalizer is used to effectively flatten the non-stationary reverberation decay that causes the signal to be non-Gaussian distributed. The normalizer only operates on the intensity data computed from the square of the reverberation envelope, and as such, a normalized form of the raw reverberation signal cannot be computed in order to test the distribution's similarity to a Gaussian. The normalized reverberation intensity is the only signal that can be tested, and this signal, calculated from the example Clutter09 reverberation time series, is shown in Figure C.8(a). The distribution of the normalized reverberation intensity is almost identical to the standard exponential pdf, as seen in Figure C.8(b) .

Note that the amplitude is *distributed* exponentially after normalization and this is not related to the seemingly "exponential" decay with time seen in the unnormalized reverberation. As in the previous section, the expected value of 1 for the standard exponential distribution is logical since the reverberation intensity signal represents SNR after normalization. This example uses real data from Clutter09 and differs from the computer generated data example in the previous section due to the presence of target echoes like those from Campo Vega's oil rig and wellhead. However, these transient signals are not plentiful enough to affect the reverberation statistics. Having an accurate assumption of the reverberation statistics allows selection of a meaningful PFA (Equation C.8), and detection of echoes using the detector in Section C.1. With the default PFA of 1.0×10^{-6}, the SNR

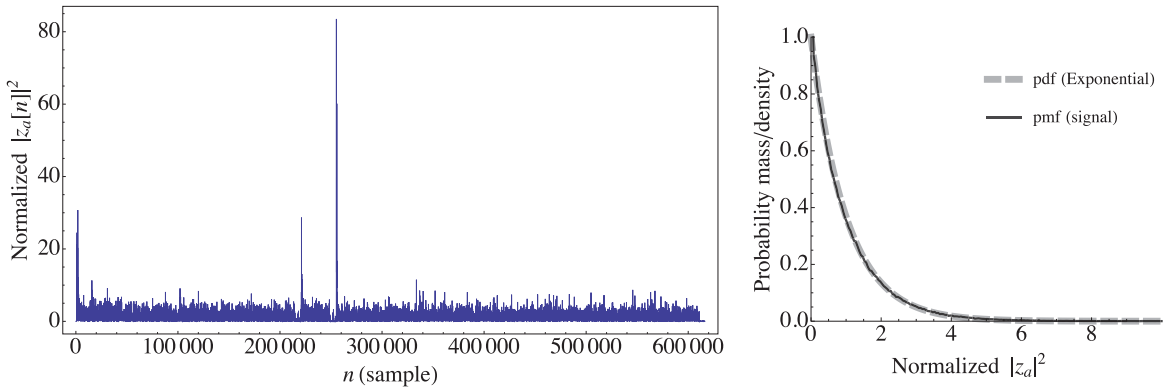

Figure C.8: *Normalized intensity time series data for a single beam recorded during the Clutter09 sea trial shown in (a), and its pmf in (b). The theoretical standard exponential pdf is also shown in (b).*

threshold is 13.82 and discounting the main blast, there are only 2 threshold exceedances in the example beam data shown in this section: the echoes from Campo Vega's oil rig and wellhead. In this example, the detector successfully identified two target echoes amidst reverberation using a constant threshold based on the assumption of an exponential reverberation intensity distribution. It should be noted that the beam time series chosen for the example was selected because it contained Campo Vega echoes, and that a total of 122 false alarms caused by clutter were detected on the other 119 beams.

This page intentionally left blank.

Annex D: Signal-to-noise ratio calculation

Figure D.1 shows an example 1.0 second echo time series, with the maximum amplitude at time t_p centered in the middle of the time series. The start and end of the echo, calculated using the Kliewer-Mertins algorithm [3], are located at times t_s and t_e, respectively.

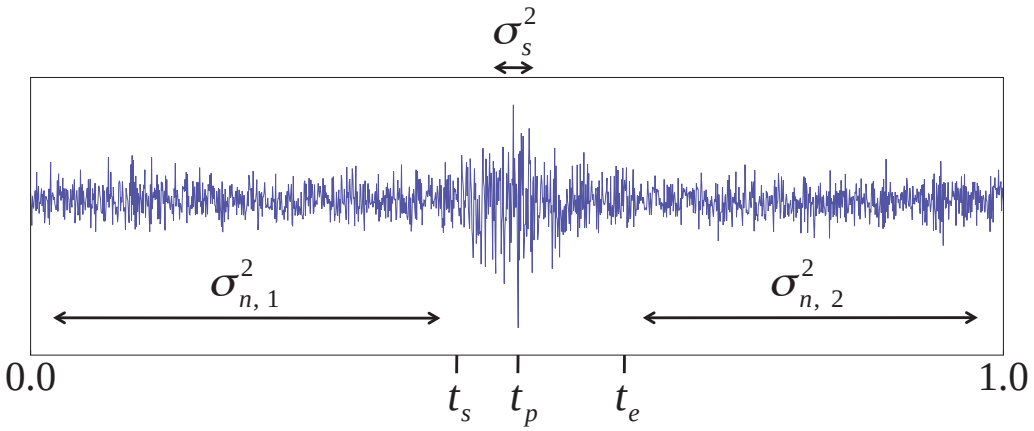

Figure D.1: *SNR calculation for an example echo with a duration of 1.0 seconds.*

The signal variance, σ_s^2, is calculated from the variance of the near-peak region: the region within 64 samples (5 ms) of the peak. This near-peak region is represented by the short double-ended arrow in the center of Figure D.1. The pre-peak noise variance, $\sigma_{n,1}^2$, is calculated using samples between the start of the snippet ($t = 0.0$ s) and the start of the echo ($t = t_s$), excluding the first and last 256 samples (20 ms). Similarly, the post-peak noise variance, $\sigma_{n,2}^2$, is calculated using samples between the end of the echo ($t = t_e$) and the end of the snippet ($t = 1.0$ s) with a 256 sample (20 ms) buffer on both ends.

Given that the noise variance should be less than the variance of the noise combined with the signal (σ_s^2), SNR is calculated as follows depending on the values of $\sigma_{n,1}^2$ and $\sigma_{n,1}^2$ relative to σ_s^2 :

If $\sigma_{n,1}^2 < \sigma_s^2$, and $\sigma_{n,2}^2 < \sigma_s^2$, then:

$$\mathrm{SNR} = \frac{1}{2}\left(\frac{\sigma_s^2 - \sigma_{n,1}^2}{\sigma_{n,1}^2} + \frac{\sigma_s^2 - \sigma_{n,2}^2}{\sigma_{n,2}^2}\right) \tag{D.1}$$

If $\sigma_{n,1}^2 < \sigma_s^2$, and $\sigma_{n,2}^2 > \sigma_s^2$, then only the pre-peak noise is considered:

$$\mathrm{SNR} = \frac{\sigma_s^2 - \sigma_{n,1}^2}{\sigma_{n,1}^2} \tag{D.2}$$

If $\sigma_{n,1}^2 > \sigma_s^2$, and $\sigma_{n,2}^2 < \sigma_s^2$, then only the post-peak noise is considered:

$$\mathrm{SNR} = \frac{\sigma_s^2 - \sigma_{n,2}^2}{\sigma_{n,2}^2} \tag{D.3}$$

Finally, if $\sigma_{n,1}^2 > \sigma_s^2$, and $\sigma_{n,2}^2 > \sigma_s^2$, the signal variance does not exceed either of the noise variances. In this case, the SNR can not be computed and the echo is removed from the dataset.

The standard conversion to decibels is shown below:

$$\mathrm{SNR(dB)} = 10 \log_{10} \mathrm{SNR} \tag{D.4}$$

Annex E: Feature list

Table E.1: *List of features ordered by discriminant score and overlap fraction ranking methods.*

Rank	Feature (discriminant score)	Feature (overlap fraction)
1	*peak loudness value*	*local min sub-band decay slope*
2	*pre-attack noise peak loudness value*	*global max sub-band attack slope*
3	*loudness centroid*	*global min sub-band decay slope*
4	*pre-attack noise integrated loudness*	*global mean sub-band decay slope*
5	*psychoacoustic bin-to-bin difference*	*peak loudness value*
6	*local min sub-band decay slope*	*pre-attack noise peak loudness value*
7	*pre-attack noise loudness centroid*	*pre-attack noise integrated loudness*
8	*max sub-band attack slope*	*loudness centroid*
9	*global min sub-band decay slope frequency*	*mean sub-band correlation*
10	*max sub-band correlation frequency*	*psychoacoustic bin-to-bin difference*
11	*global mean sub-band decay slope*	*global min sub-band decay slope frequency*
12	*global min sub-band decay slope*	*pre-attack noise loudness centroid*
13	*min sub-band correlation*	*min sub-band correlation*
14	*min sub-band correlation frequency*	*max sub-band correlation frequency*
15	*mean sub-band correlation*	*global min sub-band decay time*
16	*global min sub-band attack time*	*global min sub-band attack time*
17	*global max sub-band decay time frequency*	*local max sub-band decay slope frequency*
18	*pre-attack noise peak loudness frequency*	*min sub-band correlation frequency*
19	*peak loudness frequency*	*peak loudness frequency*
20	*local max sub-band decay slope frequency*	*pre-attack noise peak loudness frequency*
21	*global min sub-band attack time frequency*	*local min sub-band attack slope frequency*
22	*local min sub-band attack slope frequency*	*global max sub-band decay time frequency*
23	*global max sub-band decay slope*	*global max sub-band decay slope frequency*
24	*global max sub-band attack slope*	*global min sub-band attack slope frequency*
25	*local mean sub-band decay time*	*global max sub-band attack slope frequency*
26	*local max sub-band decay time*	*global max sub-band decay slope*
27	*global min sub-band decay time*	*global min sub-band attack time frequency*
28	*local max sub-band decay time frequency*	*global mean sub-band decay time*
29	*global min sub-band attack slope*	*local mean sub-band decay time*
30	*psychoacoustic MSBR*	*local max sub-band decay time*
31	*local max sub-band attack time*	*global min sub-band attack slope*

Continued on next page –

– continued from Table E.1 on previous page

Rank	Feature (discriminant score)	Feature (overlap fraction)
32	*local max sub-band attack time frequency*	*local max sub-band decay time frequency*
33	*local mean sub-band attack time*	*local max sub-band attack time*
34	*global mean sub-band attack time*	*psychoacoustic MSBR*
35	*global max sub-band decay time*	*local min sub-band attack slope*
36	*global max sub-band decay slope frequency*	*local max sub-band attack time frequency*
37	*local min sub-band attack slope*	*local mean sub-band attack time*
38	*local max sub-band decay slope*	*global max sub-band decay time*
39	*global mean sub-band decay time*	*global mean sub-band attack time*
40	*global max sub-band attack time*	*local min sub-band decay time frequency*
41	*duration*	*local max sub-band decay slope*
42	*local min sub-band decay time frequency*	*local max sub-band attack slope frequency*
43	*global max sub-band attack time frequency*	*local min sub-band decay time*
44	*local max sub-band attack slope frequency*	*global max sub-band attack time*
45	*global min sub-band attack slope frequency*	*global max sub-band attack time frequency*
46	*pre-attack noise psychoacoustic MSBR*	*duration*
47	*local min sub-band attack time frequency*	*local min sub-band decay slope frequency*
48	*local min sub-band decay time*	*local min sub-band attack time*
49	*local min sub-band decay slope frequency*	*pre-attack noise psychoacoustic MSBR*
50	*local min sub-band attack time*	*local min sub-band attack time frequency*
51	*global min sub-band decay time frequency*	*global min sub-band decay time frequency*

Note that *MSBR* stands for *maxima to spectral bins ratio*.

In training the classifier using the Clutter07 dataset, the following features were found to be redundant: *local max sub-band attack slope*, *global mean sub-band attack slope*, *local mean sub-band decay slope*, *max sub-band correlation*, *pre-attack noise psychoacoustic bin-to-bin difference*, *integrated loudness*, *local mean sub-band attack slope*.

Distribution list

DRDC Atlantic TR 2010-136

Internal distribution

3 Paul C. Hines (1 hard copy + 2 soft copies)

3 DRDC Atlantic Library (1 hard copy + 2 soft copies)

1 Stefan M. Murphy (1 hard copy)

1 H/Underwater Sensing

1 H/Technology Demonstration

1 H/Maritime Information & Combat Systems

1 GL/Maritime Environmental Awareness

1 Jeff Scrutton

1 Garfield Mellema

1 Dan Peters

1 Vincent Myers

1 Senior Military Officer

Total internal copies: 16

External distribution

Department of National Defence

1 DRDKIM
The following 6 copies sent c/o:
CFB Halifax, PO BOX 99000, Stn Forces, NS B3K 5X5

1 ADAC(A) – Commanding Officer

1 CFMWC – Commanding Officer

1 CFNOS – Commanding Officer

1 MOG5 – Commanding Officer

1 PSU HALIFAX – Commanding Officer

1 TRINITY – Commanding Officer

Canadian recipients

1 Library and Archives Canada
Attn: Military Archivist, Government Records Branch

International recipients

1 Dr. Ellen Livingston
Office of Naval Research Global
Edison House
223 Old Marylebone Road
London NW1 5TH
UNITED KINGDOM

1 Dr. James Pitton
Applied Physics Laboratory
University of Washington
1013 NE 40th Street
Box 355640
Seattle, WA 98105-6698
USA

Total external copies: 10

Total copies: 26

DOCUMENT CONTROL DATA

(Security classification of title, body of abstract and indexing annotation must be entered when document is classified)

1. ORIGINATOR (The name and address of the organization preparing the document. Organizations for whom the document was prepared, e.g. Centre sponsoring a contractor's report, or tasking agency, are entered in section 8.)

   Defence R&D Canada – Atlantic
   PO Box 1012, Dartmouth NS B2Y 3Z7, Canada

2. SECURITY CLASSIFICATION (Overall security classification of the document including special warning terms if applicable.)

   UNCLASSIFIED

3. TITLE (The complete document title as indicated on the title page. Its classification should be indicated by the appropriate abbreviation (S, C or U) in parentheses after the title.)

   Aural classification and temporal robustness

4. AUTHORS (Last name, followed by initials – ranks, titles, etc. not to be used.)

   Murphy, S. M.; Hines, P. C.

5. DATE OF PUBLICATION (Month and year of publication of document.)

   November 2010

6a. NO. OF PAGES (Total containing information. Include Annexes, Appendices, etc.)

   66

6b. NO. OF REFS (Total cited in document.)

   10

7. DESCRIPTIVE NOTES (The category of the document, e.g. technical report, technical note or memorandum. If appropriate, enter the type of report, e.g. interim, progress, summary, annual or final. Give the inclusive dates when a specific reporting period is covered.)

   Technical Report

8. SPONSORING ACTIVITY (The name of the department project office or laboratory sponsoring the research and development – include address.)

   Defence R&D Canada – Atlantic
   PO Box 1012, Dartmouth NS B2Y 3Z7, Canada

9a. PROJECT OR GRANT NO. (If appropriate, the applicable research and development project or grant number under which the document was written. Please specify whether project or grant.)

   11cb04

9b. CONTRACT NO. (If appropriate, the applicable number under which the document was written.)

   ONR Grant N00014-09-1-0426

10a. ORIGINATOR'S DOCUMENT NUMBER (The official document number by which the document is identified by the originating activity. This number must be unique to this document.)

   DRDC Atlantic TR 2010-136

10b. OTHER DOCUMENT NO(s). (Any other numbers which may be assigned this document either by the originator or by the sponsor.)

11. DOCUMENT AVAILABILITY (Any limitations on further dissemination of the document, other than those imposed by security classification.)

   (X) Unlimited distribution
   ( ) Defence departments and defence contractors; further distribution only as approved
   ( ) Defence departments and Canadian defence contractors; further distribution only as approved
   ( ) Government departments and agencies; further distribution only as approved
   ( ) Defence departments; further distribution only as approved
   ( ) Other (please specify):

12. DOCUMENT ANNOUNCEMENT (Any limitation to the bibliographic announcement of this document. This will normally correspond to the Document Availability (11). However, where further distribution (beyond the audience specified in (11)) is possible, a wider announcement audience may be selected.)

   Unlimited

13. ABSTRACT (A brief and factual summary of the document. It may also appear elsewhere in the body of the document itself. It is highly desirable that the abstract of classified documents be unclassified. Each paragraph of the abstract shall begin with an indication of the security classification of the information in the paragraph (unless the document itself is unclassified) represented as (S), (C), or (U). It is not necessary to include here abstracts in both official languages unless the text is bilingual.)

Active sonar systems are used to detect underwater manmade objects of interest (*targets*) that are too quiet to be reliably detected with passive sonar. In coastal waters, the performance of active sonar is degraded by false alarms caused by echoes returned from geological seabed structures (*clutter*) found in these shallow regions. To reduce false alarms, a method of distinguishing target echoes from clutter echoes is required. Research has demonstrated that perceptual signal features similar to those employed in the human auditory system can be used to automatically discriminate between target and clutter echoes, thereby improving sonar performance by reducing the number of false alarms.

An active sonar experiment on the Malta Plateau was conducted during the Clutter07 sea trial and repeated during the Clutter09 sea trial. Broadband sources were used to transmit linear FM sweeps (600–3400 Hz) and a cardioid towed-array was used as the receiver. The dataset consists of over 95 000 pulse-compressed echoes returned from two targets and many geological clutter objects.

These echoes are processed using an automatic classifier that quantifies the timbre of each echo using a number of perceptual signal features. Using echoes from 2007, the aural classifier is trained to establish a boundary between targets and clutter in the feature space. Temporal robustness is then investigated by testing the classifier on echoes from the 2009 experiment.

14. KEYWORDS, DESCRIPTORS or IDENTIFIERS (Technically meaningful terms or short phrases that characterize a document and could be helpful in cataloguing the document. They should be selected so that no security classification is required. Identifiers, such as equipment model designation, trade name, military project code name, geographic location may also be included. If possible keywords should be selected from a published thesaurus. e.g. Thesaurus of Engineering and Scientific Terms (TEST) and that thesaurus identified. If it is not possible to select indexing terms which are Unclassified, the classification of each should be indicated as with the title.)

active sonar
classification
pattern recognition
aural classification
detection
clutter

This page intentionally left blank.

Defence R&D Canada

Canada's leader in defence
and National Security
Science and Technology

R & D pour la défense Canada

Chef de file au Canada en matière
de science et de technologie pour
la défense et la sécurité nationale

www.drdc-rddc.gc.ca